UCLouvain

École polytechnique de Louvain

Thermal and structural properties of a polymer-based ternary system for the 3D printing of personalized pharmaceutical formulations

Auteurs : **Floriane Soenens**
Promoteurs : **Alain Jonas, Anne des Rieux**
Lecteurs : **Karine Glinel, Quentin Papeloer**
Année académique 2023–2024
Master [120] in Biomedical Engineering

Abstract

Context Advances in personalized medicine are transforming healthcare by providing treatments tailored to individual patient needs. Traditional pharmaceutical manufacturing methods are often inadequate for producing customized medications, particularly for complex cases requiring precise dosages and release profiles. The integration of 3D printing technology in pharmaceutical formulation offers an innovative approach to overcoming these limitations, enabling the creation of personalized drug delivery systems.

Objectives This study investigates the thermal and structural properties of a polymer-based ternary system suitable for the 3D printing of personalized pharmaceutical formulations. Specifically, this research focuses on the interactions between polycaprolactone (PCL) and polyethylene glycol (PEG), and examines the incorporation of aspirin as an active pharmaceutical ingredient (API) to enhance its release profile.

Experiments A series of experiments were conducted to examine the thermal and structural properties of PCL/PEG blends in order to understand their crystallization and phase separation behavior. Techniques such as differential scanning calorimetry (DSC) and fast differential scanning calorimetry (fDSC) were used to study the thermal behavior of these blends. Additionally, polarized optical microscopy (POM), scanning electron microscopy (SEM), and Fourier-transform infrared spectroscopy (FTIR) were used to analyze the morphology of PCL/PEG and PCL/PEG/aspirin blends.

Results The fDSC curves of PCL/PEG blends indicate superimposed signals of pure PCL and PEG, suggesting phase separation with minimal interaction and limited miscibility. SEM images confirmed this, showing distinct PEG phases within the PCL matrix. After PEG extraction, isolated but non-interconnected porosities were observed, questioning the effectiveness of PCL/PEG blends in drug release enhancement. In addition, the inclusion of aspirin formed a separate crystalline phase, limiting its interaction with the polymer matrix and not improving its release profile.

Discussion This thesis contributes to the understanding of biodegradable polymer blends for 3D printable drugs. Although the PCL/PEG/aspirin system showed limited drug release enhancement, it provides a foundation for future research. Efforts could focus on modifying one of the polymers to achieve better miscibility and controlled drug release.

Acknowledgements

First of all, I would like to thank my supervisors: Prof. Alain Jonas and Prof. Anne des Rieux for their help, for the time they devoted to me and for their explanations and sound advice.

I would like to thank Quentin Papeloer for his help and his support throughout my work. He devoted a lot of time to me as well, he showed me the different instruments in the lab, and guided me through this thesis.

I also thank Pascal Van Velthem for his help and the time he devoted to helping me with various manipulations and guiding me in understanding different instruments such as SEM and fDSC. I also thank Sabine Bebelman for her thorough explanations and demonstrations on the use of FTIR and Naima Sallem for her guidance with the polarized optical microscope.

I thank UCLouvain for providing me with the equipment I needed for my various experiments, for allowing me to spend five years studying within the university.

Finally, I would like to thank my family and my friends for their unwavering support throughout my studies and thesis.

Acronyms

API Active Pharmaceutical Ingredient

DSC Differential Scanning Calorimetry

FDA Food and Drug Administration

fDSC Fast Differential Scanning Calorimetry

FTIR Fourier Transform Infrared Spectroscopy

GMP Good Manufacturing Practice

$\Delta \mathbf{H}_m$ Melting enthalpy

$\mathbf{M}_w$ Molar mass

PCL Polycaprolactone

PE Polyethylene

PEG Poly(ethylene glycol)

PEO Poly(ethylene oxide)

PGA Polyglycolic acid

PLA Polylactic acid

PLLA Poly-L-lactic acid

PM Personalized medicine

POM Polarized Optical Microscopy

SEM Scanning Electron Microscopy

$\mathbf{T}_c$ Crystallization temperature

$\mathbf{T}_g$ Glass transition temperature

$\mathbf{T}_m$ Melting temperature

TE Tissue Engineering

3DP 3D printing

Contents

Chapter 1

Introduction

Personalized medicine is leading a revolutionary transformation in healthcare by providing a tailored approach to patient treatment [1]. This innovative methodology aims to customize medical treatments, drugs, and prevention strategies to fit the unique characteristics of each individual, thereby overcoming the traditional 'one size fits all' paradigm [2]. Administering the same drug and dosage to different individuals often results in varied reactions; some may suffer strong adverse effects, while others may find the treatment too mild to be effective, causing little or no therapeutic benefit. This variability can lead to further complications for patients [3].

Administering the same drug and the same dosage to different individuals is thus not optimal for treatment. It is therefore essential to develop personalized treatments tailored to the needs of each individual. Among the various options for customizing treatments, the production of tablets using 3D printing emerges as one of the most promising strategies. This technology enables the precise tailoring of medications by adjusting the shape, size, dosage, and release profile of active ingredients, thereby significantly reducing the risk of human error associated with traditional compounding methods. Therefore, 3D printing of a mixture of an active pharmaceutical ingredient (API) with one or more polymers would enable the shaping of such "tablets".

Accordingly, in recent years, the field of biomedical engineering has seen a significant increase in the use of biodegradable polymers for medical applications. Among these polymers, polycaprolactone (PCL) has gained substantial attention due to its wide availability, affordable cost, adaptability for chemical modifications, excellent mechanical stability, and compatibility with biological systems. PCL's unique properties, such as its low melting point of around 60°C and its semi-crystalline nature, make it an ideal candidate for various biomedical applications, including drug delivery systems, tissue engineering, and 3D printing. Its semi-crystalline structure, consisting of both crystalline and amorphous regions, allows for the tailoring of

physical properties through controlled crystallization conditions. However, PCL's slow biodegradation rate may pose challenges in certain applications, such as drug delivery systems.

One of the promising strategies explored in this work is the addition of polyethylene glycol (PEG) to the PCL matrix. PEG is known for its hydrophilicity, biocompatibility, and ability to act as a plasticizer, which enhances the flow properties and printability of the polymer blend. PEG is also Food and Drug Administration (FDA) approved. Incorporating PEG into the PCL matrix could potentially improve the degradation rate and drug release profile of the final pharmaceutical formulations. The biodegradability of a polymer-based material is influenced by its composition, molar mass and molar mass distribution, and degree of crystallinity. Environmental conditions such as temperature and pH, as well as the mechanical loading that the material undergoes, also play an important role in polymer degradation [4]. Therefore, the objective of this thesis is to investigate the binary mixture of PCL and PEG, aiming to advance the development of 3D printable drugs using this blend.

Our research will primarily focus on the understanding of the thermal behavior and crystallization mechanisms of the binary mixture of PCL and PEG. Understanding this is crucial for elucidating the interaction between these polymers. It will also provide information on the phase separation and morphological structure of the PCL/PEG mixture, since these two concepts are linked. Additionally, we aim to evaluate the incorporation of aspirin as the API into the PCL/PEG blend to assess its compatibility and effectiveness within the ternary system. This study will help us explore the potential of using this polymer-based ternary system for 3D printing customized tablets, aiming to revolutionize medication customization and administration for patients. Overall, our research will investigate the miscibility of PCL and PEG to determine the conditions under which they form a homogeneous mixture or not. This exploration is crucial as it allows us to assess whether the addition and subsequent extraction of PEG, under specific conditions, would induce the formation of porosities acting as a continuous network that could enhance the extraction of the drug dispersed within the blend.

To achieve these objectives, we will formulate blends of PCL and PEG, followed by the addition of aspirin. We will conduct experiments with various ratios to identify the optimal formulation at thermodynamic equilibrium.

This thesis is structured into several chapters. It first provides a review of the current state of the art of PCL/PEG blends, based on existing studies and literature. It

then delved into the objectives of this work, articulating a clear strategy to provide a comprehensive analysis of the thermal behavior and phase separation of PCL/PEG blends, as well as an in-depth examination of the morphology of these blends. Following this, the research methodology encompasses a variety of characterization techniques, including fast differential scanning calorimetry (fDSC), polarized optical microscopy (POM), scanning electron microscopy (SEM) and Fourier transform infrared spectroscopy (FTIR). These methods are then integrated to provide a comprehensive analysis of the thermal behavior and phase separation of PCL/PEG blends, as well as an in-depth examination of the morphology of these blends. Last but not least, attention is paid to mixtures in which aspirin is added in order to assess its compatibility and effectiveness within the ternary system.

Through this study, we aim to advance the field of personalized medicine by demonstrating the feasibility and effectiveness of using a polymer-based ternary system to 3D print tablets. By exploring the properties and interactions of PCL and PEG, and incorporating an API, we aim to develop a flexible and efficient method for producing customized pharmaceutical formulations. This approach could significantly enhance the precision and efficiency of pharmaceutical treatments, paving the way for more tailored and patient-specific healthcare solutions.

Chapter 2

State of the art

2.1 PCL

2.1.1 Overview

Biodegradable polymers have faced an increasing demand in medical usage over the last decades. One of such polymers is poly(ϵ-caprolactone), also called polycaprolactone (PCL). This polyester has found extensive use in the biomedical field due to its wide availability, affordable cost, adaptability for chemical modifications, excellent mechanical stability, and compatibility with biological systems [5, 6].

PCL is an aliphatic polyester belonging to the poly-α-hydroxy acid category, in the same chemical category as polylactic and polyglycolic acids. It was first synthesized in the early 1930s by ring-opening polymerization of the cyclic monomer ϵ-caprolactone using stannous octoate as catalyst. PCL is made of a chain of a repeated single-unit hexanoate sequence of $C_6H_{10}O_2$ [7]. The caprolactone monomers are connected through ester bonds between the carboxylic acid (-COOH) group of one monomer and the hydroxyl (-OH) group of another [8]. The chemical structure of PCL is shown in Fig 2.1.

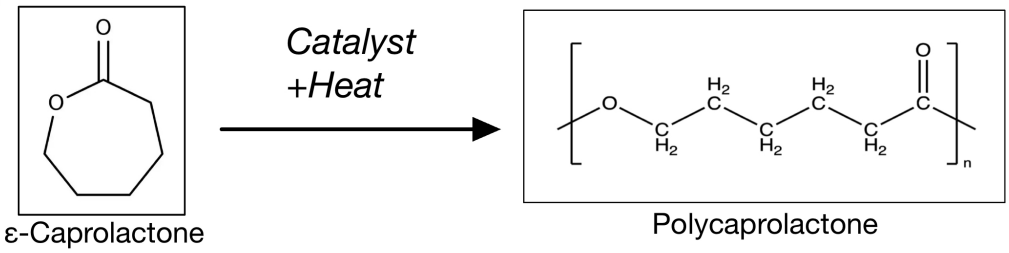

Figure 2.1: Chemical structure of PCL [8]

PCL is approved by the Food and Drug Administration (FDA), and it is biocompatible and nontoxic, meaning that it can be implanted or delivered in the human body [9].

PCL is also a semi-crystalline polymer, meaning it has a structure that includes both crystalline and amorphous regions. The chain segments in crystalline regions are regularly positioned, while in amorphous regions they have a random arrangement [8]. The ratio of crystalline to amorphous regions in PCL can be adjusted by controlling several factors, including the cooling rate during polymer solidification and various conditions such as temperature, pressure, and shear during polymer processing [10, 11]. Amorphous polymers are ideal when flexibility is needed. On the other hand, for applications that require hardness and rigidity, polymers with higher crystallinity are often the better choice. However, highly crystalline materials are also often more brittle [12]. Therefore, crystallization conditions play an important role in the final structure and physical properties of the polymeric materials [13]. In our study, it will be important to fully understand the crystallization process of our materials in order to obtain the desired structure.

Finally, PCL is a polyester with a low melting point of around 60°C and a glass transition temperature of about -60°C [14]. PCL's low melting point makes it an ideal choice for blends with active agents likely to degrade at higher temperatures, ensuring that their efficacy and stability are preserved throughout processing and application. Moreover, it is a material renowned for its exceptional versatility, allowing its chemical and biological properties, physicochemical characteristics, degradability and mechanical strength to be precisely modified. This customization enables PCL to retain its functional integrity even when subjected to harsh conditions such as intense mechanical stress [5]. Furthermore, novel PCL-based composite materials loaded with organic or inorganic fillers can help to control mechanical properties and integrate further functionalities [6]. PCL is also distinguished by its hydrophobicity, low tensile strength, and high elongation at break [9].

2.1.2 Mechanical Properties

PCL has an average density of 1.145 g/cm^3 [8]. Depending on its molar mass (M_w), PCL can be a waxy solid (M_w below several thousands) or a solid polymer (M_w above 20,000). The waxy PCL is usually used as an additive or co-component. High molar mass PCL polymer has mechanical properties similar to those of polyethylene (PE), with a tensile stress of between 12 and 30 MPa and an extension at break of between 400 and 900%. Table 2.1 outlines various properties of PCL across differing molar masses, revealing a significant dependence of these properties on molar masses. Moreover, PCL shows high-molecular-chain flexibility, coupled with

remarkable processability. Notably, it can undergo numerous processes up to 200°C without encountering thermal degradation [15].

Properties	**PCL 1**	**PCL 2**	**PCL 3**
Molar mass	37,000	50,000	80,000
Melting point (°C)	58–60	58–60	60–62
Tensile stress (kg/cm^2)	140	360	580
Elongation at break (%)	660	800	900

Table 2.1: Properties of PCL with different molar masses [15].

2.1.3 Crystallization

A molecule, material, or biomolecule (such as a protein) can exist in three different states, as illustrated in Figure 2.2. These states include the amorphous state, characterized by a lack of ordered structure; the semi-crystalline state, composed of small or large crystalline domains linked by amorphous sections; and finally, the crystalline state, characterized by a fully crystallized structure [16].

Figure 2.2: Different possible states of a material [16].

Polymeric materials typically fall into either the amorphous or semi-crystalline categories. Moreover, achieving 100% crystallinity in a polymer is unattainable in reality, but it is a very useful theoretical concept for calculating the degree of crystallinity of a polymer [16].

Polymer crystallization is a multifaceted process that can occur either during the solidification of a polymer from its molten state (cooling), when it is heated above its glass transition temperature (T_g) or during an isothermal period at a specific temperature. Throughout this process, macromolecules lose a significant amount of their kinetic energy, which dissipates into their surroundings as heat. Meanwhile, polymer molecules arrange themselves into a regular and repetitive pattern known as a crystalline structure. This structure exhibits a high degree of orderliness and gives the polymer improved mechanical properties, including increased strength and stiffness. Polymer crystallization occurs within the temperature range between T_g and the melting temperature (T_m). Indeed, near T_g, molecular motion is insufficient,

while near T_m, it is excessive. This is why intermediate temperatures (between T_g and T_m) are more suitable for crystallization, as molecular motion is neither too high nor too low for the formation of crystalline domains. Thus, ball-shaped molecule chains "stretch out" and align themselves into parallel structures composed of folded macromolecules [16, 17].

When polymers undergo crystallization from the molten state, they commonly form structures known as spherulites (see Figure 2.3 (e)), which typically exhibit spherical shapes. Spherulites are the higher-order organization of crystalline polymers, appearing as polycrystalline aggregates containing thin lamellar crystals composed of lamellar branches. Throughout the growth process, these stacked lamellae continuously spread apart and occasionally branch [13, 18]. The size of spherulites varies from micrometers to millimeters and is influenced by factors such as the polymer chain structure, crystallization conditions, and the presence of nucleating agents [13].

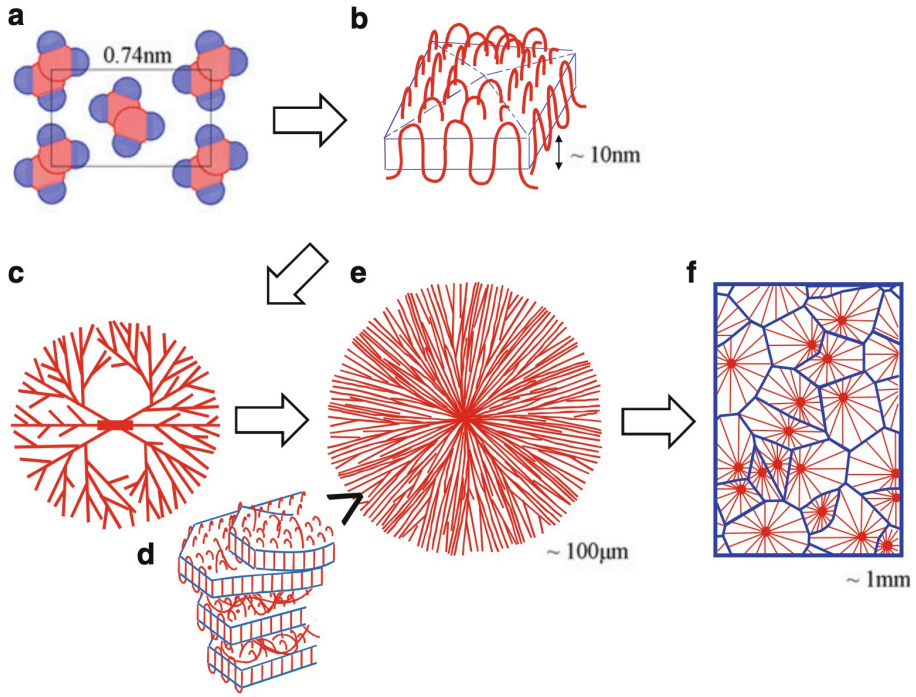

Figure 2.3: Spherulitic structure of polymers at different scale. (a) Polymer chains arranged in a three-dimensional crystal lattice. (b) Thin plate-like single crystal formed by chain folding. (c) Growing spherulite with apparent nucleus. (d) Fibrils of crystals. (e) Final spherulitic structure. (f) Crystalline structure [18].

The process of forming a crystal structure requires the presence of a crystallization nucleus, as shown in Figure 2.3c, which serves as the initial point of crystallization. This nucleus can consist of minute quantities of pre-existing crystalline polymers. Subsequently, the crystal expands outward from this nucleus until it encounters other crystals or regions of amorphously solidified material. By introducing additional

crystallization nuclei into the melt or solution, the number and size of the resulting spherulites can be controlled [17].

Then, observation at the nanometer scale reveals the smallest unit of the crystal lattice, known as the "unit cell," where atoms or molecules arrange to form a macroscopic crystal (Figure 2.3a). The thin plate-like single crystal formed by polymer chains showcases distinct features, including folds present on the upper and lower surfaces, referred to as folding surfaces. Typically, this single crystal possesses a thickness of approximately 10 nm (see Figure 2.3b). Zooming in on a red line in Figure 2.3b reveals the complex structure described in Figure 2.3a, similarly, zooming in on a red line in Figure 2.3c elucidates the structure presented in Figure 2.3b. Then, the dynamic coupling of lamellar crystals and amorphous layers to one another results in the spherulitic growth of crystalline polymers, as illustrated in Figure 2.3d. With this image, we can better understand why a 100% crystalline polymer is not feasible. Finally, Figure 2.3d shows a final spherulitic structure. This phenomenon takes place in 3D, but here it is schematized in 2D for clarity [16, 18].

The degree of crystallinity, typically falling within the range of 10% to 80%, indicates the proportion of polymer molecules that are organized in a specific manner. This degree of crystallinity determines the degree of structural ordering of a solid. The greater the crystallinity, the more uniformly aligned the polymer chains, and the more consistent and repetitive the arrangement of atoms or molecules becomes [19].

Thus, the crystallization process is a key factor in semi-crystalline polymers. Indeed, variations in factors such as the initiation of spherulitic nuclei, crystal growth speed, and lamellar thickness can induce notable shifts in the material's ultimate thermal and mechanical behavior. By manipulating variables such as crystallinity (X_c) and crystal structure, it is possible to control essential properties such as biodegradation rate and degree of permeability [20]. Indeed, increased crystallinity in PCL results in more tightly packed polymer chains within the crystalline regions, which makes it harder for enzymes to break down the material. This results in slower biodegradation. The structure and size of crystalline regions, such as spherulites, can also influence the rate of degradation; larger and denser spherulites degrade more slowly [21]. Furthermore, by increasing the crystallinity of PCL, the proportion of amorphous, more permeable areas decreases, enhancing the material's barrier properties against gases and liquids. Conversely, decreasing crystallinity increases these regions, enhancing permeability [22]. Therefore, controlling the crystallization process means that polymers can be customized with tailor-made characteristics to meet specific requirements in areas such as biomedical engineering and packaging. This strategic manipulation underlines the importance of controlling crystallization in the innovation of polymer materials

with predetermined functionalities [20].

Among all of the factors that control the crystallization process of a semi-crystalline polymer, molar mass plays a significant role. Variations in molar mass can lead to changes in chain folding, reorganization of polymer crystals, and crystallization kinetics because of the influence of end groups and entanglements [20]. Entanglement refers to the transient reticular structure formed by the cross-linking points within a polymer chain or between polymer chains. These entanglements prevent the free movement of polymer chains, thereby modifying the nature of the polymer [23]. Consequently, parameters such as crystal thickness, crystalline morphology, X_c, or equilibrium melting temperature (T_m) might be affected by the molar mass [20].

The degree of crystallinity of PCL can be computed according to the following formula:

$$X_c = \frac{\Delta H_m}{\Delta H_m^0}$$

where ΔH_m is the measured melting enthalpy and ΔH_m^0 is the theoretical melting enthalpy of completely crystalline PCL (139.5 J/g)[20].

Fernández-Tena *et al.* showed that T_m of PCL increases significantly with the molar mass, reaching saturation at M_w greater than 5.6 kg/mol. They also showed that X_c clearly depends on M_w. A maximum of X_c was observed at an optimum M_n of 2.4 kg/mol, followed by a decrease as M_w increased. This decrease can be explained by the reduction in chain diffusion due to the increase in entanglement density [20].

PCL crystalline morphology

Polarized optical microscope (POM) offers visual insights into the formation of crystalline structures, showcasing the isothermal growth of spherulites at 40°C over time. This technique provides a macroscopic view of the morphological changes during crystallization. The nucleation and growth of spherulites can be observed in Figure 2.4 [24].

In addition, Figure 2.5 shows a micrograph of melt-crystallized PCL at 30°C, revealing large spherulites with curved edges [25].

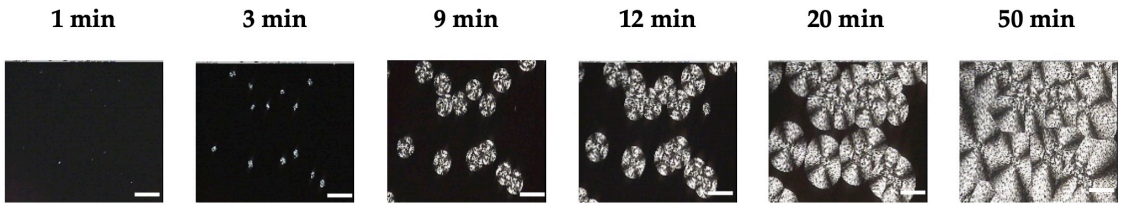

Figure 2.4: POM images showing PCL spherulitic growth over time during isothermal crystallization at 40°C (Scale bar = 100µm) [24].

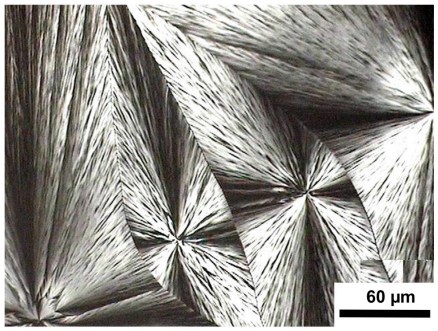

Figure 2.5: POM image showing PCL spherulites after isothermal crystallization at 30°C [25].

2.1.4 Thermal behavior of PCL

Analysis using Differential Scanning Calorimetry (DSC)

V. Speranza *et al.* conducted a study to determine the range of crystallization temperatures of PCL. They used a sample with a molar mass between 70,000 and 90,000 and subjected it to heating and cooling cycles, as shown in Figure 2.6. The tests revealed that PCL crystallizes between 44°C and 34°C, with the peak occurring at 39°C. Then, isothermal crystallization tests between 50°C and 43°C (Figure 2.7) showed that lower temperatures accelerate crystallization, resulting in sharper peaks. Specifically, PCL crystallizes more rapidly at 43°C [26].

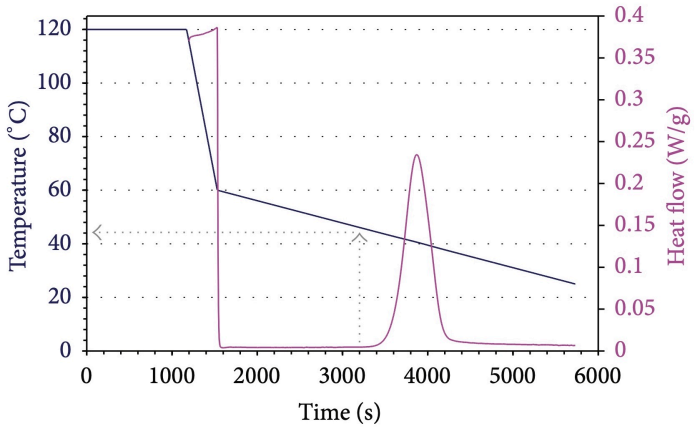

Figure 2.6: Temperature and calorimetric evolution during preliminary DSC test [26].

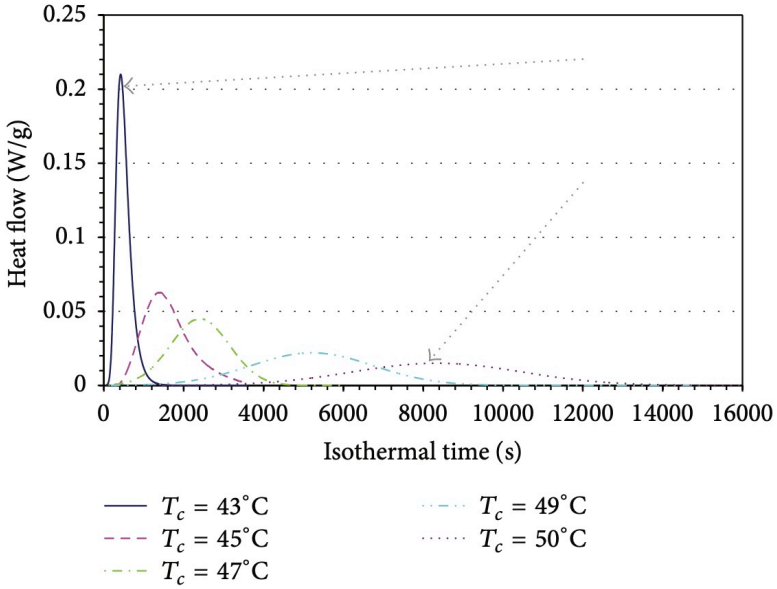

Figure 2.7: Isothermal DSC curves in the crystallization range of PCL [26].

In addition, Pires *et al.* conducted an experiment in which all the samples were heated and then cooled at rates of 5, 10, 15 and 20°C.min^{-1}. The resulting DSC curves are shown in Figure 2.8. A noticeable change in crystallization temperature can be observed as cooling rates increase. At low rates, the cooling process is slower, and crystallization therefore occurs at higher temperatures, as nucleation has more time to occur and form. Conversely, higher cooling rates lead to crystallization at lower temperatures. Therefore, a discernible temperature shift is evident based on the different cooling rates [27].

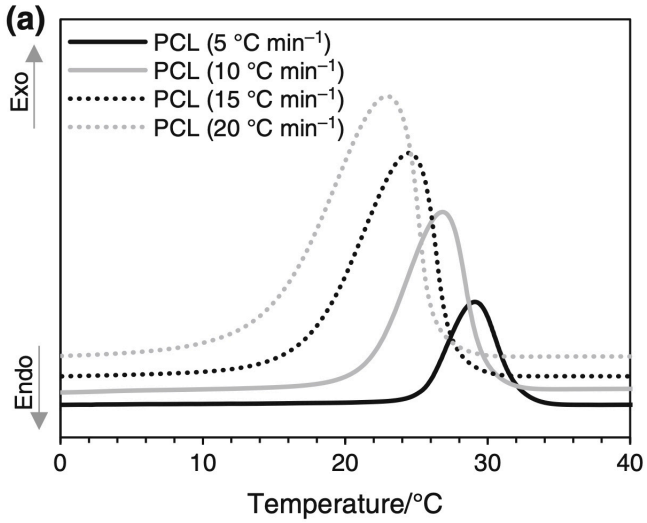

Figure 2.8: DSC curves of non-isothermal crystallization of PCL [27].

Analysis using fast Differential Scanning Calorimetry (fDSC)

With the introduction of on-chip fast scanning calorimetry, the heating rates used to analyze melting phenomena have increased considerably. It has been shown that reorganization during heating is indeed a rapid process for many polymers, which cannot be adequately captured or attenuated in standard DSC measurements. This reorganization during heating can lead to a shift in the melting peak as a function of the heating rate and can even give rise to multiple melting peaks. In conventional DSC, it is often difficult to distinguish the latter phenomenon from the melting of different crystal populations [28].

Indeed, thanks to this technique, two peaks were identified at relatively low isothermal crystallization temperatures, whereas with DSC, only one could be identified. Figure 2.9 shows the normalized heat flux (Φ_β) during post-isothermal crystallization at different temperatures (T_c). The wide range of T_c allows us to distinguish the two melting peaks and examine how T_c influences their positions. The first melting peak (T_{mo}) moves towards higher temperatures with increasing T_c, while the final melting peak (T_{mf}) is unaffected for sufficiently low T_c. These behaviors are characteristic of melting and recrystallization during heating. The initial structure resulting from isothermal crystallization at T_c melts at T_{mo}, then undergoes recrystallization and melting until final melting at T_{mf}, as shown in Figure 2.11 [28].

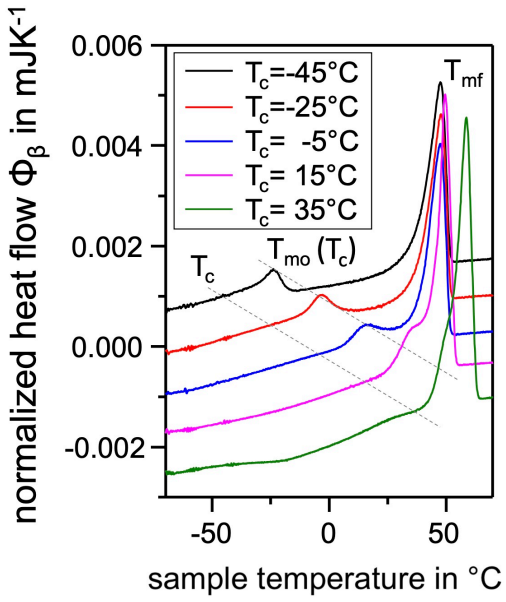

Figure 2.9: Heating fDSC thermograms of PCL measured at 100 K/s after isothermal crystallization at different T_c following the procedure in Figure 2.10. The curves are shifted vertically for clarity [28].

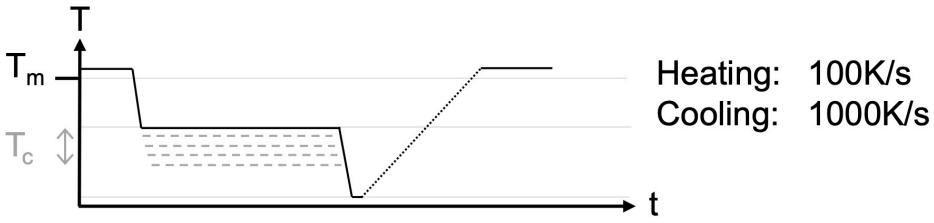

Figure 2.10: fDSC Method - Isothermal crystallization at different crystallization temperature T_c with subsequent heating run [28].

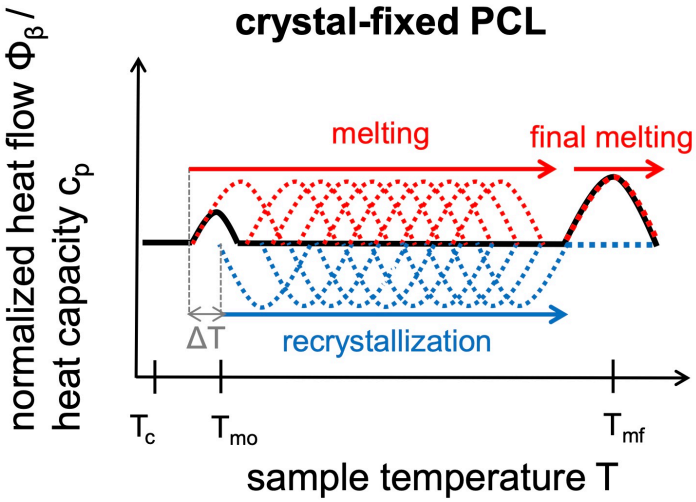

Figure 2.11: Illustration of combined melting (red) and recrystallization (blue) signals during heating after isothermal crystallization at T_c [28].

In summary, employing both DSC and fDSC techniques offers a thorough analysis of PCL's thermal behavior. DSC and fDSC offer a general understanding of crystallization temperatures and kinetics. Whereas DSC facilitates direct mass measurements, enabling quantitative analyses, fDSC prioritizes qualitative assessments. Moreover, fDSC provides deeper insights into the effects of rapid thermal changes, showing complexities like multiple melting peaks that hint at different crystalline structures or phases and preventing any rearrangement we might have during cooling. Furthermore, the results indicate that the choice of specific processing conditions, such as cooling rates or isothermal temperatures, significantly influences PCL's crystallization process. By gaining a deeper understanding of how PCL crystallizes and melts under various conditions, manufacturers can more effectively tailor the material's properties to meet the demands of specific applications.

2.1.5 Degradation rate

PCL is a slow-biodegrading polymer, typically requiring 2 to 3 years for complete degradation. Biodegradation of polymers is primarily driven by the action of microorganisms, including fungi, bacteria, and algae [29]. Biodegradation refers to the total breakdown of a product, while bioresorption involves its complete elimination from the body [7].

Polymers containing ester groups, such as PCL, can also be subject to hydrolytic degradation. This process can take place by chemical or enzymatic routes, each displaying distinct kinetics occurring under different conditions [29].
Hydrolytic degradation is an autocatalytic process in which the carboxylic acid groups produced from the hydrolyzed ester groups catalyze additional hydrolysis [30]. To be more precise, the hydrolytic degradation of implanted PCL devices involves hydrolysis of the polymer chains' ester bonds, which occurs in two distinct phases. Initially, water infiltration into the polymer bulk initiates chain scission, marking the controlled first phase. This phase follows a predictable first-order linear pattern, in which the chain length steadily decreases over time (t) due to chain scission: $M_n = M_{n,o}e^{-kt}$, where M_n represents molar mass and k is the average rate constant for chain scission [7]. This initial phase progression depends on water permeability and polymer length. Consequently, in this first phase, cleavage begins in the amorphous regions of the PCL because they are more permeable to water than the crystalline regions [31]. Subsequently, a brief second phase starts as the polymer becomes more crystalline due to the degradation of amorphous regions and reaches a chain length of a low molar mass, typically around 3000-5000 Da. This phase facilitates the diffusion of small fragments through the polymer matrix. Finally, the degradation end products (CO_2 and H_2O) are entirely eliminated from the body [7]. All degradation end products are nontoxic products, making PCL suitable for long-term implantable systems and drug delivery [32]. However, while non-enzymatic hydrolytic degradation remains the primary process in-vivo, various enzymes, particularly esterases and lipases, can also contribute to the breakdown of aliphatic polymers via enzymatic hydrolysis [29].

PCL has a strong hydrophobic nature that prevents water from seeping into it. This is chiefly attributed to the presence of five non-polar CH_2 groups in each monomer of its chain. Consequently, this hydrophobic property significantly extends the degradation time of PCL [33]. The rate of ester linkage hydrolytic degradation is influenced by numerous factors. Generally, anything that enhances water penetration speeds up hydrolysis rates [30]. Hence, for certain specific applications, PCL is used as a copolymer with other degradable polymers such as polylactic acid (PLA) and polyglycolic acid (PGA) [9]. Indeed, such polymers have a better degradation rate

compared to PCL [8]. Therefore, the process of copolymerizing or blending PCL with other polymers effectively addresses several inherent limitations of PCL, including its slow degradation properties and limited cell adhesion [34].

The rate of PCL degradation depends on factors such as moisture, temperature, and pH [33]. This phenomenon is additionally impacted by the glass transition temperature and crystallinity of the material. Elevated glass transition temperatures correspond to reduced segmental mobility and decreased available polymer free volume to allow water to penetrate. On the contrary, lower glass transition temperatures and crystallinity accelerate hydrolytic degradation by enhancing water penetration and accessibility to ester linkages within the polymer matrix [30]. Finally, faster degradation could be achieved by using an acidic or basic environment, which would stimulate the hydrolysis of the polyesters [30]. Under normal conditions, it may take several years for PCL to completely degrade [8].

2.1.6 Applications

Polycaprolactone finds applications in modeling and molding and serves as a material for rapid prototyping systems like 3D printing and fused filament fabrication [8]. Owing to its low melting temperature, PCL is easily processed by conventional melting techniques and can be filled with stiffer materials (particles or fibers) for better mechanical properties. PCL scaffolds have been used for tissue engineering of bone and cartilage [35].

Medical applications

The safety, numerous advantages, and functionality of PCL as a biomaterial have stimulated product development and prompted scientists and physicians to explore its applications in a wide range of fields, particularly biomedical. [7, 8].

Some medical applications of PCL include:

- Self-absorbing surgical sutures: Sutures were among the first devices made of synthetic absorbable polymers (including PCL), with the advantage of reproducible slow degradation in biological tissue, replacing traditional sutures like nylon or polyester. PCL sutures are flexible and have a longer self-absorption time, reducing pain and discomfort for patients [7, 8].
- Drug delivery systems: PCL serves as a drug delivery system to control the rate and location of drug release within the body due to its high permeability to many drugs, excellent biocompatibility, slow biodegradability, and bioresorbability [7,

8]. PCL drug delivery systems can be used to treat chronic diseases such as cancer or diabetes [8]. Indeed, many drugs have been encapsulated in PCL microspheres, in particular: anticancer, antipsychotic, non-steroidal anti-inflammatory, and others [7].

- Skin and bone grafts: PCL is used in implants in various tissues, extensively in 3D scaffolds to promote repair and regeneration in bone, skin, or other tissues, and in the engineering of autologous grafts [7]. PCL is used as a skin graft to cover wounds or skin defects. On the other hand, it is employed as a bone graft to regenerate damaged or lost bone tissue [8].

- Tissue engineering (TE): TE explores various methodologies, including the use of scaffolds generated by 3D printing, an area that is rapidly advancing in research and practical applications. PCL emerges as a pivotal material in this context due to its advantageous physicochemical attributes, such as a low melting point, and mechanical properties, including moldability and durability. In 3D printing, structures are crafted through the sequential deposition of layers via computerized control. This technology holds immense potential in tissue repair and organ replacement, representing a highly promising therapeutic avenue that is increasingly transitioning from theoretical exploration to practical implementation [7].

2.2 PCL/PEG blends

PCL demonstrates high compatibility with various substances, making it an excellent candidate for blending with other polymers. Indeed, the presence of CH_2 and C=O groups allows PCL to interact favorably with other polymers. When PCL is combined with a hydrophilic, safe, and biodegradable polymer such as polyethylene glycol (PEG), the resulting blends are expected to have enhanced biodegradability and hydrophilicity. This improvement makes them suitable for short-term pharmaceutical delivery applications [36].

2.2.1 PEG properties

PEG is a synthetic, FDA-approved polyether compound characterized by its biocompatibility and hydrophilicity. Predominantly utilized within the medical domain, PEG also finds application in the chemical and industrial sectors [37]. PEG is also known as polyethylene oxide (PEO), depending on its molar mass. PEG tends to refer to shorter polymers, while PEO refers to longer polymers [38]. Its molecular structure is represented in Figure 2.12.

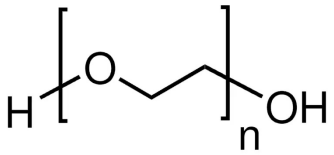

Figure 2.12: Molecular structure of PEG [39].

PEG, as previously mentioned, is a highly biocompatible material known for its water solubility and low toxicity, making it a versatile compound in various applications [40]. Its solubility in water is a critical property that varies with the molar mass of PEG; as the molar mass increases, its solubility in water and other solvents decreases. Consequently, PEGs with lower molar masses are preferred for applications requiring higher solubility [41]. Its high hydrophilicity not only contributes to its solubility but also enables it to decrease the contact angle significantly when blended or copolymerized with hydrophobic polymers, enhancing their interface and interaction with water [42].

Moreover, despite the differences in physical properties such as viscosity, which are influenced by the chain length, the chemical properties of PEG and PEO remain nearly identical across different molar masses [38].

The physical state of PEG varies with its molar mass (M_w). PEGs with a M_w ranging from 100 to 700 exist as liquids at room temperature. On the other hand, those with M_ws between 1000 and 2000 are in the form of soft solids, while PEGs with a M_w exceeding 2000 are characterized as hard crystalline solids with a melting point of approximately 63°C [43]. By combining PEGs of varying molar masses, it is possible to modulate the glass transition temperature and the melting temperature of the material. For example, the glass transition temperatures of PEG 4000, 6000 and 20,000 are -34.6°C, -22.7°C and -22.37°C respectively, with corresponding melting points of 67.7°C, 58.7°C and 51.6°C [42].

Furthermore, PEG's role extends beyond medical applications; it is a primary polymeric additive in membrane formation and serves as a coating material in biotechnical applications. This wide range of uses underscores the importance of understanding the unique properties of PEG and how they can be optimized for specific applications, highlighting its invaluable role in science and industry [44].

2.2.2 PCL/PEG blends

Recently, PCL/PEG blends have been investigated for the formation of biodegradable membranes and controlled drug delivery [44]. The appeal of using these materials lies in their complementary properties. Indeed, PEG can improve the water solubility of the final blend, while PCL provides mechanical strength and controlled biodegradability. The presence of PEG plasticizes the amorphous regions of PCL, enhancing the flexibility of PCL/PEG scaffolds [45].

Crystallization and Phase Behavior

The crystallization behavior of PEG and PCL in blends is a focal point of study due to their close phase transition temperatures (T_c, T_m and T_g) [46]. The complexity of crystallization arises from their similar melting points, which suggests a potential for simultaneous crystallization when cooled from the melt. However, altering the crystallization conditions, such as temperature and composition, can result in significant differences in crystallization rates [36]. In addition, by conducting experiments where the system was rapidly cooled below the melting point of PCL from a molten state, Chuang *et al.* demonstrated the competitive dynamics between liquid-liquid phase separation and crystallization within the polymer blend [47].

Another study revealed that in a PCL/PEG blend containing 50% PEG by weight, a distinct crystallization behavior develops at lower temperatures (30°C). Indeed, the blend exhibits a two-step crystallization process, where PCL spherulites dominate

the structure while PEG is segregated outside, along with amorphous PCL. At a higher temperature (40°C), both PEG and PCL crystallize simultaneously, but PEG segregates into the PCL structure at the submicrometer scale, illustrating the complex interplay between phase separation and crystallization dynamics. In simple terms, the authors suggested in their study that phase separation occurs at 30°C and 40°C. At 30°C, it takes place outside the spherulites (interspherulitic segregation), while at 40°C, it takes place inside the spherulites (interspherulitic segregation) [36]. The authors explained this behavior by the existence of a miscibility window for PCL/PEG blends, characterized by an upper critical solution temperature (UCST) [47]. Indeed, at 30°C, phase separation occurs in the melt, resulting in PCL spherulites and later PEG crystallization on their boundaries. At 40°C, rapid cooling prevents phase separation, causing internal phase separation during crystallization, forming PEG nodules within PCL spherulites [36].

Microstructural Observations

Through advanced techniques like AFM-IR, the distribution and structural characteristics of PCL and PEG within the blends have been elucidated. For example, the AFM-IR spectra of neat PCL and neat PEG, crystallized isothermally at 30°C, provide insight into the molecular interactions within the blends (Figure 2.13). Indeed, overlapping bands can be observed between the two spectra, as well as bands specific to each of the two spectra. The band at 1103 cm^{-1} shows a high intensity in the PEG spectrum but a lower intensity in the PCL spectrum. Similarly, the band at 1720 cm^{-1}, indicating the stretching vibration of the carbonyl group, shows significant intensity in the PCL spectrum, whereas it is absent in the PEG spectrum. These bands allow us to probe the distribution of PEG and PCL in the blend [36].

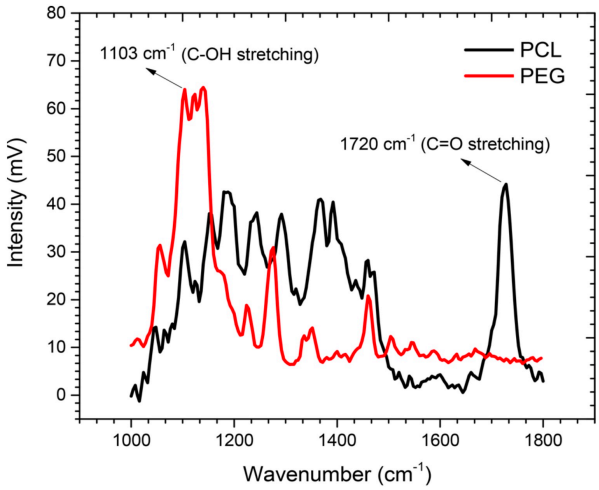

Figure 2.13: AFM-IR spectra of neat PCL and neat PEG, isothermally crystallized at 30°C in the 1000-1800 cm^{-1} range [36].

At a temperature of 40°C, AFM images (Figure 2.14) show phase separation during the initial crystallization stages, revealing numerous nodules varying in size from several hundred nanometers to one micrometer (Figure 2.14b). These solid nodules primarily consist of PEG, as can be seen from the green areas showing their weak absorption at 1720 cm^{-1} (Figure 2.14a) and the pronounced absorption at 1103 cm^{-1} (Figure 2.14c) [36].

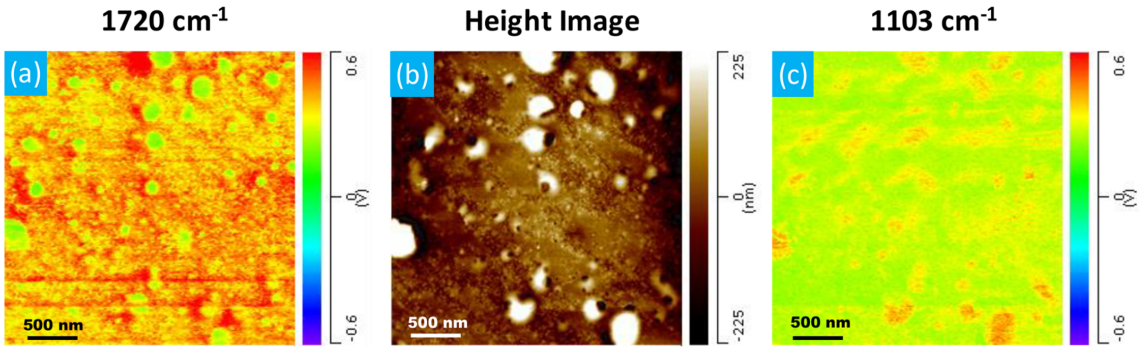

Figure 2.14: PCL/PEG (50/50) blend, quenched after 10 min at the crystallization temperature of 40 °C from the melt: (a) chemical image of the 1720 cm^{-1} band, (b) AFM image, and (c) chemical image of the 1103 cm^{-1} band [36].

The study of PCL/PEG blends reveals how different factors, such as the properties of the materials and the way they are processed, influence their use in areas such as drug delivery and biodegradable materials. Research by Phuong Nguyen and others focuses on how temperature, molar mass, and blend composition influence the behavior of these blends, including their phase behavior and crystallization rate, and ultimately their effectiveness for their intended uses [36].

2.3 Aspirin as the active ingredient

Acetylsalicylic Acid (ASA), more commonly known as aspirin, is one of the oldest and most widely used medications in the world, with an annual consumption of 40,000 tonnes, serving as an anti-inflammatory, antipyretic (fever reducer), and analgesic (pain reliever) [48]. This medication plays an essential role in over-the-counter and prescription medicines because of its versatility in treating pain, fever, inflammation, and as an antiplatelet agent to prevent blood clots, strokes, and myocardial infarction's (heart attacks) [49].

2.3.1 Synthesis of aspirin

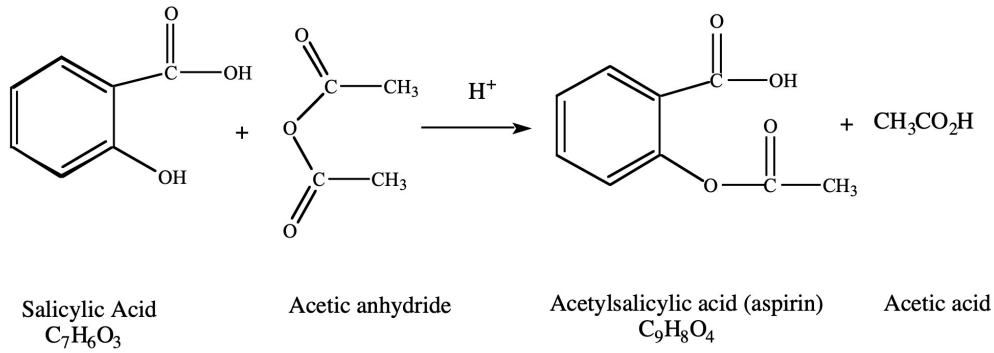

Figure 2.15: Aspirin synthesis [50].

The synthesis of aspirin is a chemical process known as esterification. In this reaction, salicylic acid is combined with acetic anhydride, leading to a transformation where the hydroxyl group (R-OH) in salicylic acid is converted into an ester group ($R\text{-}OCOCH_3$). This conversion results in the creation of aspirin and a side product, acetic acid (Figure 2.15). To facilitate this reaction, sulfuric or phosphoric acid is used as a catalyst to accelerate the process [51].

2.3.2 Properties of aspirin

Aspirin is distinguished by its chemical composition, having the formula $C_9H_8O_4$, with a molecular mass of approximately 180.159 g/mol [52]. It is characterized by its white, crystalline powder form, which is typically odorless and tasteless, making it distinct in appearance. Notably, aspirin only emits an acetic acid odor when exposed to humid air, which is explained by the breakdown of its components into acetic and salicylic acids under such conditions [53]. Furthermore, aspirin crystals are needle-shaped, making them easy to distinguish under the microscope [54].

Physically, aspirin has a melting point of about 136°C and it is a substance soluble in water, ethyl ether, ethanol, and chloroform [49, 53]. These properties, combined with its abundance, low cost, non-toxic nature, and its remarkable thermal stability, make aspirin a preferred choice in various applications.

Despite its numerous benefits, including pain relief, inflammation reduction, and lowering the risk of heart attacks and strokes, aspirin can cause side effects such as stomach ulcers and gastrointestinal bleeding. However, the advantages of aspirin often outweigh these risks, underscoring the continued prevalence of its medical use [53].

Regarding toxicity, the threshold for acute aspirin toxicity is generally set at more than 150 mg per kg of body weight, with symptoms ranging from ringing in the ears to abdominal pain and accelerated breathing [55].

2.4 3D printing for personalized medicine

2.4.1 Personalized medicine

Personalized medicine (PM) is at the forefront of a wave of healthcare transformation, offering a personalized approach to patient treatment [1]. This cutting-edge methodology aims to tailor medical treatments, drugs, and prevention strategies to the unique characteristics of each individual, overcoming the traditional 'one size fits all' paradigm [2]. Indeed, administration of the same drug and dosage to different people has resulted in different reactions. Some people may have stronger reactions, leading to adverse effects, while others may find the effects too mild, resulting in little or no therapeutic benefit. This variability can lead to further complications for patients [3]. The basis of PM is a detailed understanding of a patient's genetic make-up, which enables healthcare professionals to select the most appropriate drugs, determine optimal dosages, and design tailor-made treatment plans [2]. The move towards personalized medicine is similar to choosing perfectly fitting shoes, recognizing the uniqueness of each individual while meeting their specific health needs. Imagine a healthcare system where diagnoses are rapidly determined on the basis of an individual's unique genetic profile and where treatments are specifically designed to be most effective for the individual, thereby reducing or even eliminating side effects [2, 56].

Personalized medicine holds the promise to greatly enhance and sustain healthcare systems. Over the past decade, it has garnered considerable interest due to significant advancements in technology that enable a deeper understanding of individual biological variations. However, personalized medicine faces several obstacles and challenges that must be addressed for its full integration into healthcare practices. The complexity involved in adapting personalized medicine approaches to the European Union's healthcare frameworks and other health systems worldwide has slowed their broad implementation. Despite these challenges, personalized medicine offers a range of potential advantages, such as reducing the risk of adverse drug reactions, maximizing the effectiveness of treatments, supporting the stability of healthcare systems, and accelerating the pace of pharmaceutical research and development [57].

2.4.2 Benefits of 3D printing

As said previously, the ability to tailor treatments to each patient's unique needs is at the heart of the concept of personalized medicine. 3D printing (3DP) technology offers a transformative solution to this challenge by enabling the on-demand manufacture of medical tablets with precise dosages, formulations and release profiles. Unlike

traditional mass manufacturing processes, 3DP enables the production of small batches of medicines tailored to individual patients, offering unprecedented flexibility and customization. In addition, studies by Ahmed et al. and Tayeb et al. further emphasize the significance of 3D-printed pharmaceutical systems for personalized treatment, showcasing the potential of this technology in addressing complex medical conditions and enabling the creation of multi-compartment tablets loaded with formulations of various drugs. These advancements highlight the versatility and adaptability of 3DP in pharmaceutical applications [58].

In addition, the drug development process has traditionally focused on the general needs of patient groups, often adopting a one-size-fits-all approach to the manufacture of solid oral medicines. This approach is inadequate, especially for groups like pediatric patients, whose treatment requirements vary based on age and body weight [59]. Attempts to address this issue through manual tablet division or the use of dividers have proven ineffective, lacking conformity to pharmacopoeial standards [3]. In response, 3DP offers a flexible solution, enabling the creation of drugs tailored to individual patient needs, leading to enhanced safety, accuracy, and customization compared to manual methods [60].

Furthermore, traditional pharmaceutical compounding often struggles to meet Good Manufacturing Practice (GMP) standards, resulting in issues such as uneven product quality and dosage strength. However, the automation of the compounding process using 3D printers in clinical pharmacies can address these challenges by minimizing contamination and producing customized drugs in terms of size, shape, color and flavor with superior quality and accurate dosing, improving patient satisfaction [58].

2.4.3 Challenges and limitations of 3D printing in the pharmacological field

3DP in PM offers the potential to tailor drug dosages to patients' genetic profiles, enhancing treatment effectiveness. However, integrating this technology into clinical pharmacy faces multiple challenges, including technical aspects, quality control, safety, and regulation. Moreover, navigating through legal privacy concerns, regulatory standards, financial considerations, and practical implementation obstacles requires collaborative efforts among scientists, healthcare providers, and policymakers. Although completely replacing traditional medication delivery with 3D printing may not be feasible or necessary, there is significant potential for these approaches to coexist and complement each other in therapeutic practices, gradually progressing towards significant breakthroughs [61].

Conducting quality control assessments on 3D-printed tablets at hospital dispensaries or pharmacies could cause delays, especially considering the specific challenges associated with certain printing techniques. For instance, tablets printed through extrusion methods might shrink or become deformed during the drying process. Additionally, the frequent issue of printer nozzle clogging can lead to structural and surface irregularities in the final product. Addressing these challenges requires the optimization of various manufacturing parameters [3, 61].

Another challenge in implementing 3DP in clinical settings is the lack of regulatory guidelines from the FDA and other authorities for the production of personalized 3D printed products in hospitals and pharmacies. Concerns about GMP compliance to prevent cross-contamination and ensure batch consistency have also been raised [58].

3DP technology, though promising, faces cost challenges compared to traditional manufacturing methods. For instance, the production costs of Spritam®, a drug developed using 3DP, are higher than their counterparts. In PM, additional expenses like genetic testing and staff training could further raise costs, potentially making 3D printed tablets unaffordable for some patients [58, 61]. Finding suitable materials for optimal drug release and quality is another hurdle. These materials must be medication-compatible, biocompatible, biodegradable, and suitable for 3DP without producing toxic substances during processing [3, 61].

Finally, while the use of 3DP in PM in hospitals and pharmacies remains largely theoretical due to regulatory and financial challenges, the prospect of directly sending customized clinical data to a 3D printer for the creation of personalized drugs is very promising and operationally viable [61].

Chapter 3

Objectives and strategy

3.1 Objectives

Tailoring treatments to the specific needs of patients is becoming more and more of a reality (withdrawal, doses adapted as closely as possible to requirements, etc.). Within this context, the use of 3D printing technology to produce customized tablets represents a promising strategy. Indeed, this technology makes it possible to produce customized medicines by adapting the shape, size, dose and release profile of the active ingredient and reducing the risk of human error that may be associated with magistral preparations. This research focuses on the thermal and structural properties of a polymer-based ternary system for the 3D printing of personalized pharmaceutical formulations. A polymer-based ternary system with an active ingredient as the third component of the system could be an innovative solution and improve personalized treatment. Indeed, the combination of two polymers with the inclusion of an active ingredient in the system could offer potential advantages in regulating the drug release profile, thus optimizing therapeutic outcomes.

Initially, we will formulate blends of polycaprolactone (PCL) and polyethylene glycol (PEG) as the base materials for these tablets. A primary objective of this research is to thoroughly investigate the binary mixture of PCL and PEG. This examination will include detailed thermal and microscopic analyses to understand the mixture's properties comprehensively. Indeed, in the context of blends, it is essential to investigate the phase separation and the crystallization mechanisms that occur in the blend. This understanding is important to regulate both the morphological structure and the final properties of the blend. Thus, our analysis will focus on the crystallization behavior of the PCL/PEG blends, considering various compositions of PCL and PEG to identify optimal formulations. Following this, our focus will extend to a ternary mixture, incorporating aspirin into the PCL/PEG base to form a PCL/PEG/aspirin blend. Aspirin will be incorporated as the active pharmaceutical

ingredient (API) to evaluate its compatibility and effectiveness within the blend.

The choice of PCL is justified by its FDA approval status, established utility in medical applications, and desirable thermal properties, including suitable melting and glass transition temperatures for 3D printing processes. PEG, meanwhile, was chosen for its solubility in water and transition temperatures compatible with those of PCL. In addition, PEG can act as a plasticizer and therefore improve the flow properties of the material, making it easier to extrude and giving better printing results. Aspirin is chosen as the API due to its affordability, safety profile, and widespread use in pharmaceutical research, making it an ideal candidate for pioneering new methodologies in tablet fabrication. In this context, aspirin is destined to demonstrate concepts rather than be a commercial product destined for pharmacy shelves. It serves as a reference to facilitate the development of innovative approaches. Chosen for its effectiveness and thermal stability, aspirin is ideal for high-temperature processes such as 3D printing, where other agents could degrade. Its stability is particularly remarkable in the PCL/PEG mixture, making it ideal for initial testing before applying these methods to other, more relevant active ingredients.

Therefore, the main objective of this study is to comprehensively explore the interactions and phase separations between PCL and PEG, with the aim of determining whether the inclusion of PEG would enhance the release of the API. In other words, our goal is to investigate the miscibility of PCL and PEG to determine the conditions under which they form a homogeneous mixture or not. This exploration is pivotal as it allows us to assess whether, under specific conditions, the addition of PEG would induce the formation of porosities acting as a continuous network that could enhance the extraction of the drug dispersed within the blend. Another master's thesis is currently in progress and focuses on the 3D printing of PCL/aspirin tablets. However, our interest lies in gaining further insights into the PCL/PEG/aspirin blend, which first requires a thorough understanding of the PCL/PEG mixture.

Finally, through this study, we aim to advance the field of personalized medicine by demonstrating the feasibility and effectiveness of using a polymer-based ternary system to 3D print tablets. This could revolutionize medication customization and administration for patients.

3.2 Strategy

The research will involve a detailed examination of various PCL/PEG mixtures. The initial phase of sample preparation involves the production of PCL/PEG films at specific concentrations. This process begins with the dissolution of PCL and PEG

in chloroform, followed by the evaporation of the solvent to form the films. The casting solvent is used to produce homogeneous thin films from the polymer blends studied. These films can then be subjected to various physical analyses to assess their thermal and structural properties. For some experiments, these films need to be crystallized. The crystallization of polymer films at controlled temperatures enables the formation of crystalline structures in the material to be studied without the effect of the solvent. Indeed, film crystallization will promote a more regular and precise molecular organization at the crystalline scale, providing a better understanding of the material's properties and performance in a wide range of applications. This is done using hot presses that heat the films to 80°C, melt the polymers, and then allow crystallization at a temperature of 25°C for up to four hours. In addition, for other experimental purposes, it is necessary to extract PEG from crystallized films using distilled water, as PCL is insoluble in water. The extraction of PEG will allow us to observe precisely where and how the PEG has been mixed with the PCL. This is particularly valuable as, in certain cases and depending on the method used, distinguishing between the two components of a mixture can sometimes be challenging.

To ascertain the optimal proportion for our blend, we will conduct experiments with various ratios, aiming to identify an optimal configuration. This study will thus focus on PCL/PEG blends containing 5, 10, 15, 20, 30 and 50 percent by weight (wt.%) PEG and a blend containing 60 wt.% PCL, 20 wt.% PEG and 20 wt.% aspirin.
Achieving thermodynamic equilibrium will ensure reproducible distribution of the active ingredient throughout the filament, which is crucial to ensuring the same therapeutic dose in each printed tablet. In addition, achieving thermodynamic equilibrium has a significant influence on the microstructure and porosity of tablets produced by 3D printing. These characteristics are essential for determining the rate of dissolution and subsequent release of the active ingredient into the body. An optimal equilibrium is essential for modulating drug release kinetics and is also beneficial for enhancing drug stability.

To understand the miscibility of PCL with PEG, we will examine the blends mentioned above (with the exception of the blend with aspirin) using fDSC. These mixtures will be stabilized at temperatures ranging from 50°C to -40°C. This temperature range was chosen because 50°C corresponds to a temperature close to the melting temperature, while -40°C is close to the glass transition temperature of PCL and PEG, and as explained before, the crystallization of polymers occurs between the glass transition and the melting temperature. The blends were then quenched rapidly to -90°C. This approach gives us a better understanding of the state of the mixture at the desired temperatures, as it prevents any rearrangement of the blend.

Then, to provide valuable information about solid-state structure and the spatial organization of polymer chains, our approach is to first use a polarized optical microscope to examine the crystalline structures in the uncrystallized films before and after PEG extraction. This analysis will allow us to determine the distribution of PEG in the films. In addition, SEM will be used to obtain a more accurate observation of the morphology and spatial distribution of polymer chains on the surface of the films. Non-crystallized and crystallized PCL/PEG films, before and after PEG extraction, will be thus analyzed by SEM, as well as crystallized PCL/PEG/Asp films before and after PEG extraction. This technique offers high contrast, enabling exceptional clarity of surface detail. For this method, we will use films that have been crystallized at 25°C as that is the optimal crystallization temperature.

Finally, Fourier-transform infrared spectroscopy was used on crystallized and non-crystallized films to assess the miscibility of PEG in PCL. FTIR mapping will therefore be realized on the surfaces of PCL/PEG films, and correlations with fDSC and SEM results will be established.

Chapter 4

Materials and methods

4.1 Materials

Poly(caprolactone) PCL pellets with a M_w of 50 000 were purchased from NaturePlast. Poly(ethylene glycol) PEG powder with a M_w of 100 000 g/mol (PEG 100K) was obtained from Sigma-Aldrich. Chloroform ($CHCl_3$) was also purchased from Sigma-Aldrich and used as acquired.

4.2 Blend preparation

Different PCL/PEG blend films were prepared. Six different concentrations by weight were used: 5%, 10%, 15%, 20%, 30% and 50% of PEG and one PCL/PEG/aspirin film was prepared with a concentration of 60% of PCL, 20% of PEG anf 20% of aspirin. In total, seven films were prepared. For the sake of clarity, PCL/PEG blends will be written as such in the remainder of this thesis: PEG5, PEG10, PEG15, PEG20, PEG30, PEG50. To obtain a homogeneous mixture of both the 2-component and the 3-component, we will use a solvent. Given that PCL, PEG, and aspirin are all soluble in chloroform, it serves as the ideal solvent for this purpose. The polymers were placed in a beaker to obtain a total of 200mg of polymer for the PCL/PEG blends and 300mg for the PCL/PEG/Asp blends. Table 4.1 shows the quantities in milligrams of each component present in each blend. A magnetic bar was placed inside the beaker, and 5 ml of chloroform was added in order to have a concentration of 40 mg/ml. To prevent evaporation of the chloroform, the beaker was closed with aluminum foil and placed on a magnetic stirrer with a stirring speed of 500 revolutions per minute (rpm). The mixture was left on the stirring plate until the polymers were completely dissolved. Once a homogeneous solution was obtained, it was poured into a 60 mm diameter glass Petri dish to form a round, uniformly flat film. The film was left to cure overnight to form a thin layer. This layer was carefully removed from its mold and stored in a plastic Petri dish under ambient conditions for later examination. The entire procedure was carried out at room temperature.

Blends	Mass of PCL (mg)	Mass of PEG (mg)	Mass of aspirin (mg)	Total mass (mg)
PCL/PEG 5%	190	10	0	200
PCL/PEG 10%	180	20	0	200
PCL/PEG 15%	170	30	0	200
PCL/PEG 20%	160	40	0	200
PCL/PEG 30%	140	60	0	200
PCL/PEG 50%	100	100	0	200
PCL/PEG/Asp 60%/20%/20%	180	60	60	300

Table 4.1: Proportion of each component in each blend.

4.3 Isothermal crystallization

The isothermal crystallization of the films was performed by a thermal process. The thermal treatment takes place in two stages. Firstly, the polymers are melted at 80°C and then the temperature is set at a specific temperature for crystallization. Here, we set the crystallization temperature at 25°C (room temperature). To maintain a homogeneous environment, two thin metal sheets, each covered with aluminum foil, were used. On one of these sheets, a layer of Kapton was placed to facilitate removal of the samples after processing. A mold, made from thicker aluminum foil, was then placed on top of the Kapton layer. In this mold, small fragments of a PCL/PEG film pre-prepared by solvant casting were arranged in several layers. Next, another sheet of Kapton was placed over the mold, and the second sheet of metal was placed over the entire assembly to embed the mold configuration. A diagram illustrating this configuration is shown in Figure 4.1.

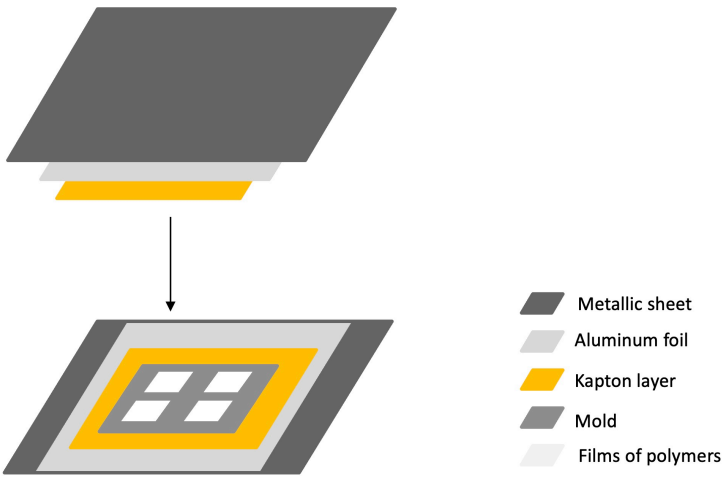

Figure 4.1: Assembly scheme for crystallization process.

Thus, once the assembly has been placed in the hot-pressing machine set to 80°C, the polymers are left to melt for 5 minutes. At the end of the 5 minutes, in order to eliminate any air bubbles that might have formed between the layers, the pressure exerted by the machine on the assembly was gradually increased to 5 MPa and then reduced to 0 MPa. This process was repeated 10 times. The assembly was then left at room temperature (approximately 25°C) and held at this temperature for 4 hours to allow the polymer blend to crystallize.

Afterwards, the top metal sheet along with the Kapton layer were removed, and the now-crystallized films were gently peeled away. These films were subsequently stored in small Petri dishes containers under ambient conditions until they were ready for further processing.

4.4 Extraction method

In order to extract the PEG from the prepared films, distilled water was used. Beakers were filled with distilled water, into which a sample of each mixture was immersed. These beakers were then placed on a stirring plate operating at 130 rpm and maintained at room temperature. The films were immersed first for 2 hours and then for 24 hours. After the initial 2-hour period, the water was replaced to prevent PEG saturation. The samples were then dried for 24 hours at room temperature.

4.5 Characterization techniques

4.5.1 Differential Scanning Calorimetry (DSC)

A differential scanning calorimeter DSC1 (Mettler Toledo, Greifensee, Switzerland) was used to determine the glass transition temperature (T_g), the melting temperature (T_m) and the optimal crystallization temperature (T_c) of the samples. DSC analyses were carried out under nitrogen gas with sample masses of about 12 mg, that were put in an aluminum pan. All the experiments were conducted in nitrogen (flow rate 50mL/min) in order to prevent oxidative degradation.

The first method is shown in Figure 4.2 and was used to find T_g and T_m of PCL and PEG. The investigated temperature range of the first heating was between -80°C and 80°C at a rate of 10 K/min, followed by a cooling from 80 to -80°C at -10 K/min, and a second heating was performed from -80 °C to 80°C at a rate of 10 K/min.
The second procedure illustrated in Figure 4.3 was intended to find the optimal crystallization temperature of PCL. Thus, at first, PCL sample was heated (H_1) to 80°C at a rate of 10 K/min. Following this, the sample was maintained at 80°C,

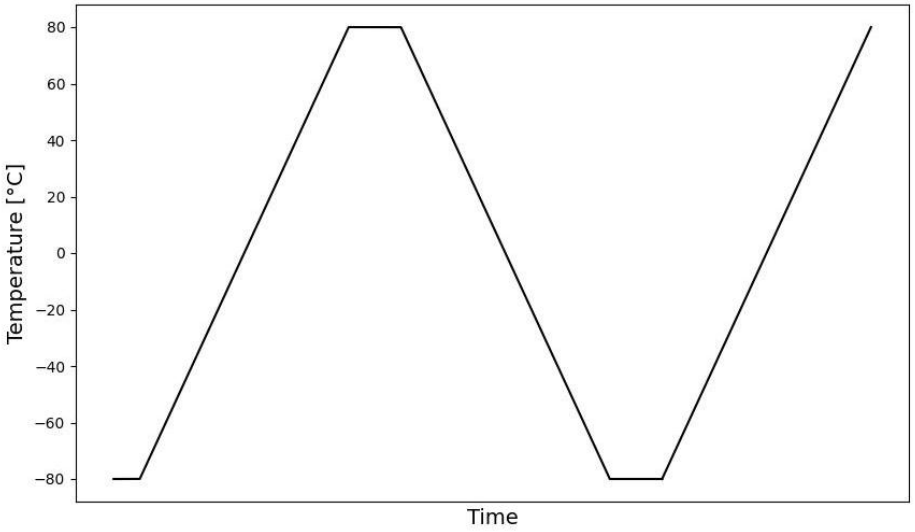

Figure 4.2: DSC temperature ramps used to determine T_g and T_m of PCL and PEG.

above the melting temperature of PCL, for 5 min to eliminate any residual crystals, thus resetting PCL thermal history. Subsequently, the sample was quenched at 10 K/min from its molten state to a temperature T_{hold}, at which the polymer state was examined. This temperature was then held for 30min. T_{hold} varied from 40°C to 10°C by steps of 10°C. The sample was then subsequently cooled from T_{hold} to 0°C at a rate of 10 K/min. Finally, the sample was heated from 0°C to 80°C (H_2) at 10 K/min to explore the evolution state.

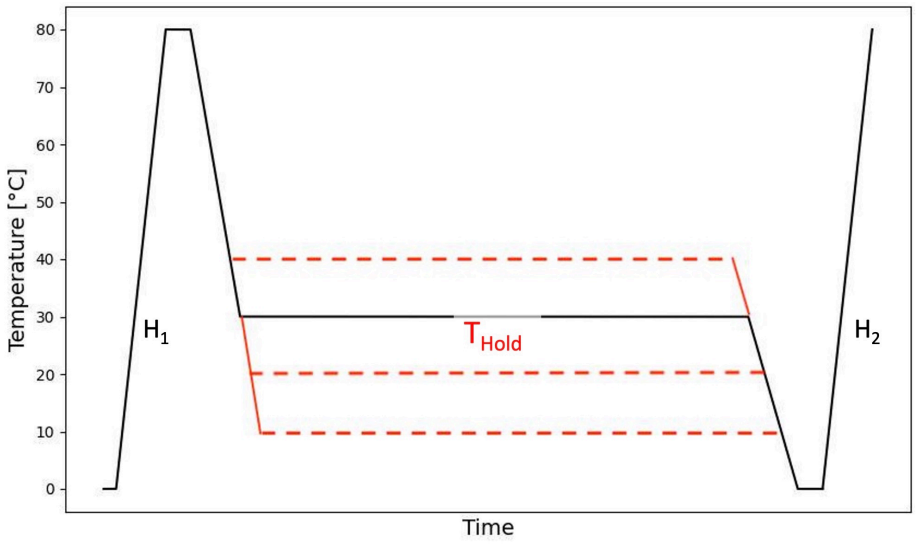

Figure 4.3: DSC temperature ramps used to find the optimal crystallization temperature of PCL.

4.5.2 Fast Differential Scanning Calorimetry (fDSC)

fDSC analysis was used to measure the glass transitions of the blends ($T_{g,blend}$) and to investigate the isothermal crystallization of the blends at different temperatures. fDSC crystallization experiments were performed on a Flash DSC 1 instrument from Mettler-Toledo connected to an intercooler and nitrogen purge gas. The calorimetric chip-sensor was conditioned three times and corrected one time prior to use according to the standard procedure. Then, a small piece of the films (see Section 4.2 for film preparation) or extruded pellets (ca. a few hundreds of ng) were cut with a razor blade and manipulated with a paintbrush hair under a microscope. The fDSC samples were too small for their mass to be measured. The samples were then placed at the center of the fDSC chip.

The temperature ramps used in fDSC are described in Figure 4.4. At first, for the isothermal crystallization tests, the thermal history of all samples was reset by rapidly heating (H_1) them to 100°C at a rate of 1000 °C/s. Following this, the samples were maintained at 100°C, above the melting temperature of PCL, for 1 second to eliminate any residual crystals. Subsequently, the samples were quenched at 1000 °C/s from their molten state to a temperature T_{hold}, at which the blend state was examined. This temperature was then held for 30s. T_{hold} was varied from 50°C to -40°C for each sample to observe the evolution of the blend state in this temperature range. The samples were then subsequently cooled from T_{hold} to -90°C at a rate of 1000°C/s, effectively "freezing" their equilibrated states. Finally, the samples were heated from -90°C to 100°C (H_2) at 2000°C/s to explore the evolution state. The glass transition temperatures (T_g) as well as the melting peaks (T_m) were defined as the midpoint of the specific heat jumps and the maximum of the endothermic peaks in the fDSC curves, respectively.

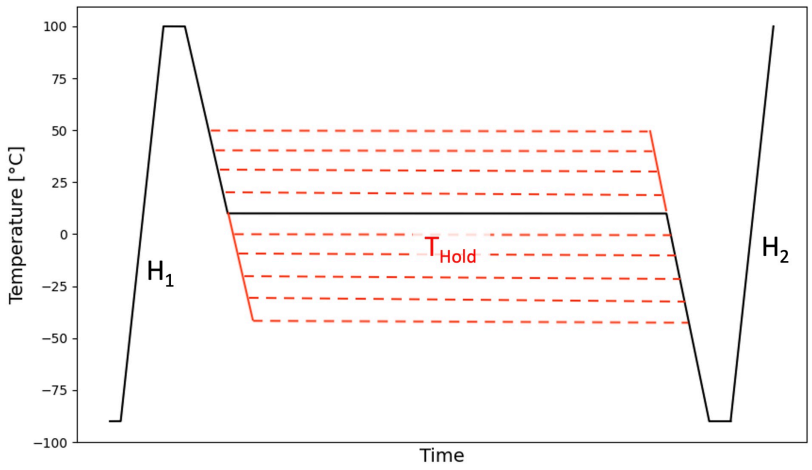

Figure 4.4: fDSC temperature ramps used to determine the phase diagram of PCL/PEG blends.

4.5.3 Polarized Optical Microscopy (POM)

PCL, PEG and composites were observed by polarized optical microscopy (POM) on an AX70 microscope from Olympus equipped with a charge coupled device (CCD) camera. The neat PCL, PEG and composites to be observed were placed between two glass slides at ambient temperature. Objectives with magnifications of x10 and x50 were used. The CCD camera was used to capture images of the samples.

4.5.4 Scanning Electron Microscopy (SEM)

The surfaces of PCL/PEG films with different PEG concentrations were analyzed by scanning electron microscopy (SEM) on a JEOL 7600F instrument (JEOL Ltd., Tokyo, Japan) operated at 1.5 kV at room temperature. A thin layer of gold (around 10 nm) was coated by sputtering on the surface of the composite specimens with a sputter coater (Ted Pella, Cressington 208HR High Vacuum Turbo Sputter Coater), prior to observations, to be electrically conductive.

4.5.5 Fourier Transform Infrared Spectroscop (FTIR)

FTIR was carried out by a NicoletTM iNTM 10 infrared microscope from Thermo Fisher Scientific in attenuated total reflectance mode (ATR). The FTIR absorption spectrum of PCL, PEG and PCL/PEG films were recorded in the wavenumber range from 2200 to 600 cm^{-1} with a spectral resolution of 4 cm^{-1}.

4.6 Writing Aids

In this work, ChatGPT, an AI language model developed by OpenAI, was used to assist in rewriting and refining certain sentences. This tool was employed to enhance the clarity, coherence, and overall quality of the text [62].

Chapter 5

Result and discussion

PCL and PEG are both biocompatible and are already widely used in the biomedical sector. Both exhibit semi-crystalline properties. Therefore, phase separation can occur either through liquid-liquid phase separation, similar to classical amorphous polymer blends, or through the crystallization of one component resulting in a liquid-solid phase separation process. To study the binary mixture of PCL and PEG, pure PCL, pure PEG and five different blend compositions (PEG5, PEG10, PEG15, PEG20, PEG30, and PEG50) were studied, with all films being produced using the same methodology.

5.1 Thermal behavior

To fully understand the behavior of PCL/PEG blends, it is essential to understand the different states that PCL and PEG can assume depending on the temperature they encounter. This understanding can be facilitated by fast differential scanning calorimetry (fDSC). Indeed, using fDSC with extremely fast cooling rates, samples can be instantaneously quenched from high temperatures (100°C) to low temperatures (-90°C), allowing snapshots of the state of the blend to be captured without the interference of (re)crystallization during cooling and subsequent heating. This method is essential for exploring temperatures that are typically inaccessible due to rearrangements during heating.

First, the fDSC procedure described in Figure 5.1 was applied on a sample of pure PCL and on blends of PCL and PEG with 10 and 20 wt% of PEG. This procedure was realized to assess the impact of cooling rates, which is an essential step in finding the optimal parameter to prevent interference from (re)crystallization during cooling. The samples were heated to 100 °C and then cooled to -90°C at different cooling rates of 10, 50, 100, 200, 500, 1000 and 2000°C/s. Finally, the samples were heated (H_1) to 100°C at 2000°C/s. The optimal parameter for the cooling rate was identified when neither endothermic nor exothermic peaks were observed during cooling. Indeed, the absence of crystallization or melting peaks indicates that the material did not have sufficient time to reorganize into another structure, which is crucial for our subsequent analysis.

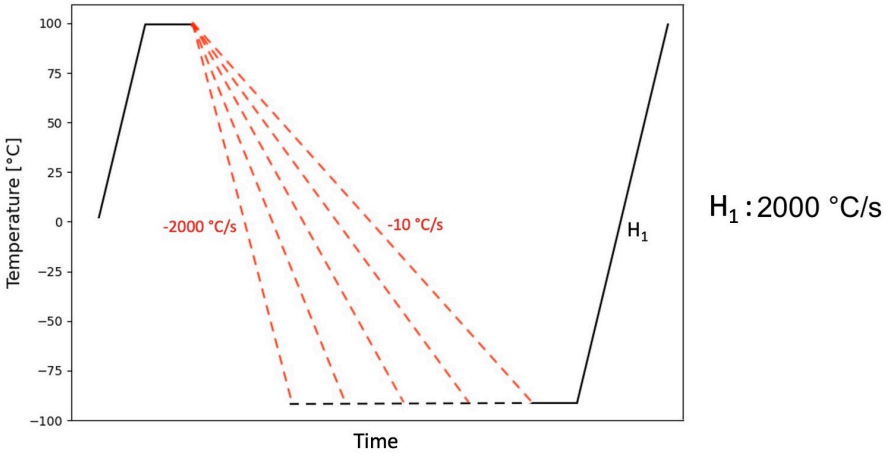

Figure 5.1: fDSC method used to assess the impact of cooling rates

Therefore, we found that the optimal parameter was a cooling rate of 1000 °C/s, as shown in Figure 5.2. Indeed, this Figure shows that PCL, PEG10 and PEG20 do not undergo reorganization at this cooling rate since neither endothermic nor exothermic peaks were observed.

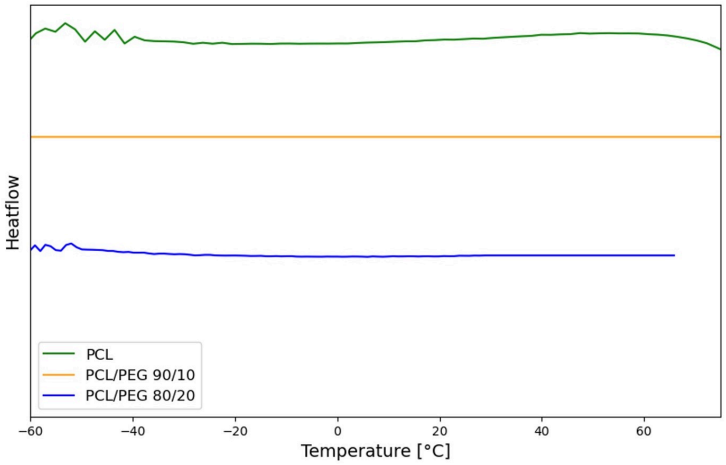

Figure 5.2: fDSC cooling curves of pure PCL, PEG10 and PEG20 at 1000°C/s (the curves have been shifted vertically for clarity).

5.1.1 PCL and PEG thermal behavior

The fDSC procedure outlined in Figure 4.4 was initially used to analyze samples of pure PCL and pure PEG. The curves shown in Figures 5.3 a and b represent the second heating curves (H_2) for pure PCL and pure PEG, respectively. Within those two graphs, T_{hold} ranges from 50°C (upper curve) to -40°C (lower curve), with an increment of 10°C. As the main objective of this investigation is to interpret the interactions between PCL and PEG within the blend, we will focus on the key trends observed in the fDSC curves.

First, in Figure 5.3a we can see that PCL undergoes different behaviors depending on T_{hold}. Indeed, at higher temperatures (50°C and 40°C), PCL does not undergo crystallization. Subsequently, PCL undergoes isothermal crystallization from T_{hold} 30°C to -40°C. Indeed, melting peak(s) can be observed during H_2 but no crystallization peaks are observed. Therefore, if no crystallization occurred during heating, this means that it took place during isothermal equilibration. On top of that, an additional melting peak emerges while decreasing T_{hold} starting from T_{hold} -20°C. This particular PCL crystallization peak exhibits a "shoulder" shape rather than a typical peak structure, which becomes more pronounced as T_{hold} decreases. This behavior is characteristic of melting and recrystallization during heating as already explained in part 2.1.4. The initial structure resulting from isothermal crystallization at T_{hold} melts in the first melting peak, then undergoes recrystallization and melting until final melting, as shown in Figure 2.11 [28]. Moreover, the comparison of the temperatures of the second melting peak of pure PCL for different isothermal temperatures reveals a significant shift. Indeed, the melting peaks shifted from approximately 60°C to 35°C as T_{hold} decreased. The downward shift of $T_{m,PCL}$ as T_{hold} decreases can be attributed to PCL crystallizing in lamellae of different thicknesses at different T_{hold} temperatures.

Then, looking at pure PEG curves depending on T_{hold} (see Figure 5.3b), two behaviors can be seen. First, at higher temperatures (from 50°C to 30°C), PEG undergoes cold crystallization, and thus it means that it does not crystallize during the isotherm. Then, at lower temperatures (T_{hold} ranging from 20°C to -40°C), there is no more cold crystallization and thus PEG undergoes isothermal crystallization since a melting peak is present during heating. The crystals formed during isothermal crystallization are not so different from those formed during cold crystallization since the melting peaks are quite similar. Indeed, PEG exhibits a really small shift in its melting temperatures for the different isothermal temperatures, with melting peaks consistently occurring between 50°C and 56°C.

Figure 5.4 illustrates the melting peaks temperatures observed at various isothermal temperatures for pure PCL, pure PEG, and their blends. Here, we specifically focus on the two pure components, represented by green circles for pure PCL and red crosses for pure PEG. This graph allows us to better observe that, due to the shift in the melting peaks of PCL, T_m of PCL and PEG become increasingly distinguishable as T_{hold} decreases. In contrast, distinguishing between the melting points of PCL and the melting points of PEG is much more challenging at higher temperatures (T_{hold} values between 0 and 30°C).

Moreover, T_g may serves as useful indicator for elucidating a crucial factor in

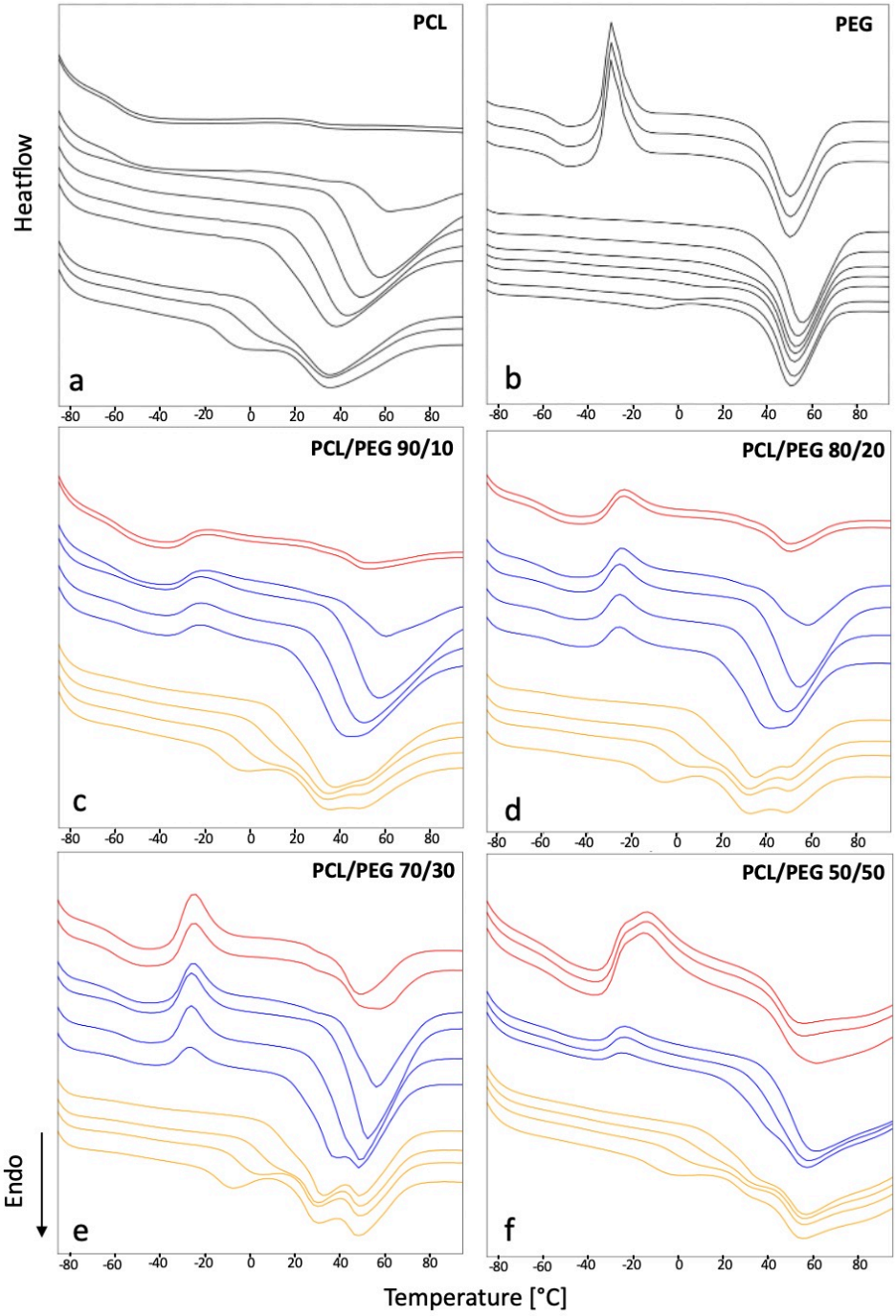

Figure 5.3: fDSC second heating curves (H_2) for pure PCL (a), pure PEG (b) and a series of PCL/PEG blends: 90/10 (c), 80/20 (d), 70/30 (e) and 50/50 (f) with T_{hold} varying from 50°C to -40°C by steps of 10°C from top to bottom in a panel (the curves have been shifted vertically for clarity). The colors are used to identify different categories of behavior. **Type I** (red): liquid-liquid phase separation. **Type II** (blue): liquid-solid or liquid-liquid phase separation where PCL crystallizes during isothermal equilibration and PEG crystallizes during heating. **Type III** (yellow): liquid-solid or liquid-liquid phase separation where by PEG and PCL crystallize during isothermal equilibration.

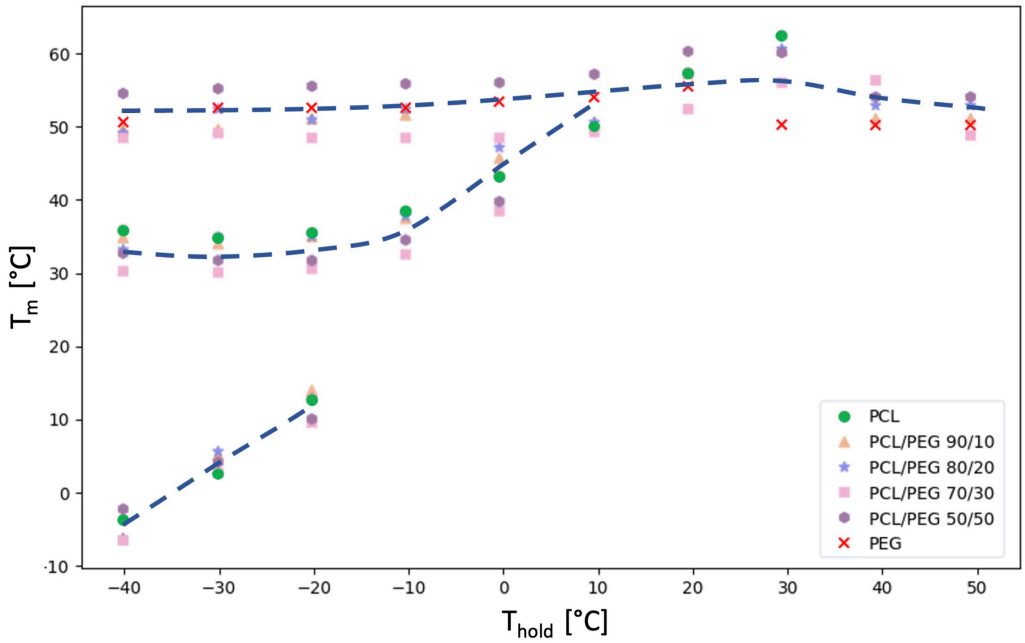

Figure 5.4: Melting temperatures of neat PCL, neat PEG and PCL/PEG blends of the following compositions: 90/10, 80/20, 70/30, 50/50 versus equilibration temperatures (T_{hold}) ranging from -40°C to 50°C. The dotted blue lines are manually placed as visual guides showing three regimes.

comprehending blend behavior. In fact, the T_g of a blend lies between the T_g values of its components. When a blend displays a single T_g, it usually indicates a high degree of miscibility between its components. On the other hand, the presence of different T_gs in a blend indicates the presence of different phases within it. In our case, as previously mentioned, both PCL and PEG exhibit remarkably close T_g values, as illustrated in Figure 5.5. The detection of T_g is limited to the isothermal curves between 50°C and 30°C. This restriction is due to the fact that at lower isothermal temperatures, the detectability of T_g decreases due to the reduced specific heat jump caused by the crystallinity of PCL and PEG. Thus, since the T_g values of PCL and PEG are very similar, detecting significant changes in T_g resulting from the mixing of these two components proves to be quite challenging. Consequently, drawing conclusive insights from T_g data is not feasible in this context.

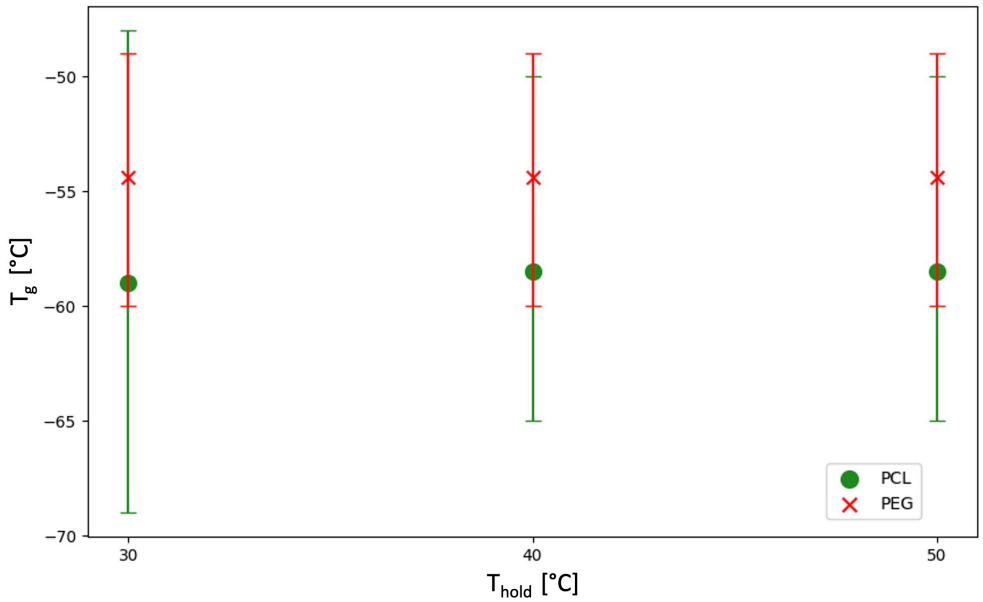

Figure 5.5: T_g of neat PCL and neat PEG for T_{hold} ranging between 30°C and 50°C. Errors bars correspond to the temperature range between the onset and offset temperatures of the specific heat jump.

The proximity of the transition temperatures of PCL and PEG adds complexity to our understanding of PCL/PEG blends. Indeed, as mentioned previously, PCL and PEG exhibit melting temperatures of approximately 60°C and 65°C, respectively, and glass transition temperatures of around -60°C and -67°C, respectively [63]. This is why it is so important to analyze very finely the results of the fDSC curves for PCL and PEG and compare them to identify similarities and differences. This comparative analysis is crucial for gaining insight into the behavior of the blends. Thus, in our analysis of PCL/PEG blends, we will explore not only their melting temperatures but also the occurrence of cold and isothermal crystallization phenomena.

5.1.2 Analysis of fDSC curves of PCL/PEG blends

Having analyzed the thermal properties of pure PCL and pure PEG, we now turn our attention to the thermal behavior of blends made from these polymers. Figure 5.3c, d, e and f shows the second heating curves (H_2) for PEG10, PEG20, PEG30 and PEG50 respectively. In each graph of Figure 5.3, T_{hold} varies from 50°C (upper curve) to -40°C (lower curve), with a 10°C increments. The strategic use of distinct colors for the traces helps readers to discern and classify the different samples according to their observed behaviors. This systematic categorization facilitates further exploration of the phase separation dynamics that will be studied in a later section.

General analysis

Figure 5.3 demonstrates consistent general behavior across blends of various compositions under different isothermal temperatures (T_{hold}). Indeed, we can see a consistent pattern of cold crystallization for the blends occurring within the same temperature range for T_{hold} from 50°C to 0°C. This figure also reveals a close similarity in the melting peak temperatures across the blends, indicating a uniform thermal behavior for blends with different compositions.

Figure 5.4 presents, as said previously, the melting peak temperatures for pure PCL, pure PEG, and their blends at various isothermal temperatures. This makes it easier to compare the melting behavior of these materials. Three behaviors, represented by dotted blue lines, can be identified on this graph. Two lines are tracing the position of PCL melting peaks, represented by green dots. Indeed, as previously indicated, a second melting peak appears for PCL as T_{hold} decreases, hence the presence of a second line. However, it is important to notice that the position of the points defining the second line are subject to greater error, as they represent not-well-defined peaks (the shoulder-shaped peaks). Care must therefore be taken not to draw hasty conclusions. The third line traces the location of PEG melting peaks, represented by red crosses. Therefore, the graph makes it easier to see which peaks correspond to PCL or PEG in the different blends. Then, a notable observation that has already been mentioned is the shift in the crystallization peak of PCL from approximately 60°C down to 35°C as T_{hold} decreases. This shift is critical for distinguishing between the PCL and PEG peaks at lower isothermal temperatures. From T_{hold} above 0°C, it becomes challenging to differentiate between the peaks of PCL and PEG since the points begin to overlap, as illustrated in Figure 5.4, emphasizing the complexity of their interpretation.

The curves in Figure 5.3 and Figure 5.4 suggest that the two components, PCL and PEG, exhibit limited miscibility. This conclusion comes from the observation that the blend curves appear to be simple superpositions of the individual curves of PCL and PEG, with no significant differences that would indicate interactions between the two components and, consequently, miscibility.

More in-depth analysis

Having established a general understanding of how PCL/PEG blends behave under various conditions, we will now go deeper into this analysis by examining the fDSC curves presented in Figure 5.3. Our strategy to thoroughly understand the phase behavior of these blends involves multiple steps. First, we will analyze the heating

phase after the isotherm to identify any crystallization or melting peaks. If any critical information is missing from the heating phase curves, we will then investigate what occurs during the isothermal phase. This approach will allow us to comprehensively study the phase behavior of PCL/PEG blends and draw accurate conclusions about their properties and interactions.

First, an initial behavior implies a sequence of cold crystallization followed by a melting peak, and it is characterized by red curves in Figure 5.3. PEG10 demonstrates this initial behavior for T_{hold} of 50°C and 40°C. This behavior is also evident for PEG20 and PEG30 at the same isothermal temperatures. Additionally, in the case of PEG50, this behavior is observed over a wider T_{hold} range from 50°C to 30°C.

Then, a second behavior characterized by blue curves also involves cold crystallization, although the melting peaks are significantly higher than those observed in the primary behavior (red curves). PEG10, PEG20 and PEG 30 display this second behavior for T_{hold} between 30°C and 0°C. This behavior is also retrieved for PEG50 for T_{hold} between 20°C and 0°C.

Finally, a third behavior, characterized by yellow curves, exhibits two distinct melting peaks in the four different mixtures, with the gradual appearance of a third peak as T_{hold} decreases. This time there is no cold crystallization. PEG10, PEG20, PEG30 and PEG50 exhibit this third behavior for T_{hold} between -10°C and -40°C.

In the red curves (first behavior), the cold crystallization and melting correspond to those of PEG. This information comes from the analysis of pure PCL and pure PEG fDSC curves (Figure 5.3a and b). Indeed, pure PCL never undergoes cold crystallization at the isothermal temperatures of the red curves. On the contrary, PEG undergoes cold crystallization from T_{hold} 50°C to 30°C. It can therefore be deduced that only PEG undergoes crystallization during heating in the red curves of the different blends. Then, to get a better idea of the similarities and differences in the red curves between the different blends and the pure components, we have put together the curves of pure PEG and the blends for isothermal temperatures of 50°C and 40°C (see figure 5.6). This Figure shows H_2 only for T_{hold} 50°C as we have the same result at T_{hold} 40°C. These temperatures correspond to the common temperatures of the red curves between the different blends. Thus, we can see that the cold crystallization and melting peaks of PCL/PEG blends align well with those of pure PEG as shown with the black dotted lines for T_{hold} 50°C. However, a shift to the right is observable for PEG crystallization during heating in PEG50 (purple curve) compared to pure PEG and the other blends. More precisely, it seems that there are two crystallization peaks and two melting peaks. One peak likely corresponds to PEG, as observed in the curves

of other blends, while the other could be attributed to PCL. Typically, pure PCL does not crystallize at this temperature, but it is possible that the prior crystallization of PEG facilitates the formation of PCL crystals. This suggests that there may be a weak nucleating effect on the crystallization of PCL thanks to PEG.

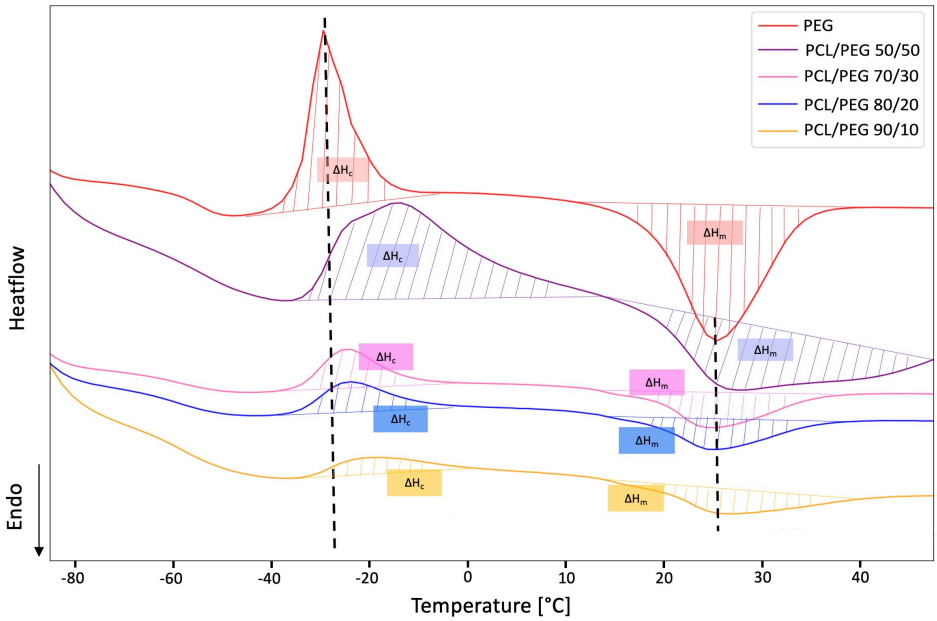

Figure 5.6: fDSC second heating curves (H_2) for the comparison of pure PEG and PCL/PEG blends for T_{hold} at 50°C (the curves have been shifted vertically for clarity). The dotted black lines are visual guides to see the alignment of crystallization and melting peaks between PEG and the different blends. ΔH_c and ΔH_m are represented for the different curves.

Furthermore, evaluation of the crystallization and melting enthalpies of the red curves in the different blends shows that the crystallization and melting enthalpies for each curve individually are remarkably similar, meaning that whatever crystallized during heating melted immediately afterwards, as shown in Figure 5.6. Indeed, as the table 5.1 shows, the absolute differences between crystallization enthalpy (ΔH_c) and melting enthalpy (ΔH_m) are small for the different red curves in the four different blends.

Several hypotheses can be put forward to explain the fact that these differences are not equal to zero. Firstly, one possible explanation could be attributed to measurement errors. It is sometimes difficult to accurately capture the area under the curve for enthalpy calculations, particularly when baseline definitions are not clear. Secondly, there is a plausible scenario where a small fraction of PCL may have crystallized during the isotherm phase and melted simultaneously with PEG during the subsequent heating phase (H_2). Although this hypothesis might not be

	T_{hold} [°C]	$\lvert\Delta H_c\rvert$ [J.g^{-1}]	$\lvert\Delta H_m\rvert$ [J.g^{-1}]	$\lvert\Delta H_c - \Delta H_m\rvert$
PCL/PEG 90/10	50	36	50	14
	40	38	50	12
PCL/PEG 80/20	50	50	58	8
	40	49	58	9
PCL/PEG 70/30	50	42	52	10
	40	46	57	11
PCL/PEG 50/50	50	132	141	9
	40	132	143	11
	30	162	165	3

Table 5.1: Values of the crystallization enthalpy (ΔH_c), the melting enthalpy (ΔH_m) and the absolute difference between ΔH_c and ΔH_m for the red curves in the four different blends.

visibly evident on the isotherm curve (see Figure 7.1 in Appendices), it remains possible. Lastly, another hypothesis suggests that a small portion of PEG could have crystallized during the isothermal phase and melted concurrently with the PEG that crystallized during H_2. This hypothesis gains credibility compared to the previous hypothesis, considering that under these conditions, neat PCL curves do not display crystallization. Nonetheless, the blend may still exert an influence, with PEG potentially acting as a nucleating agent for PCL, thus supporting the second hypothesis.

DSC measurements can be carried out in addition to fDSC measurements to see which polymer crystallizes first, as we cannot see it clearly in fDSC. The DSC measurements indicate that PEG can indeed act as a nucleating agent, as it crystallizes more rapidly than PCL. By analyzing the DSC isothermal curves of both PCL and PEG with the DSC procedure outlined in Figure 4.3, we gained a clearer understanding of the crystallization process during isothermal equilibration. Figure 5.7 shows the DSC curves of PCL during the isothermal equilibration (T_{hold}) between 40°C and 10°C. We can observe that PCL crystallizes during isothermal equilibration at holding temperatures of 40°C and 30°C. At 40°C we can observe a slow crystallization as the crystallization peak is very wide. Then, as we decrease T_{hold}, the crystallization is getting faster and faster. At T_{hold} of 10°C and 20°C, PCL crystallizes very rapidly. Indeed, crystallization no longer takes place during isothermal equilibration, but during the first cooling phase before isothermal equilibration, as shown in Figure 5.8. For those isothermal temperatures, we can thus observe a crystallization peak at 24°C.

When we conducted the same experiments with PEG, we observed no crystallization during isothermal equilibration (see Figure 7.2 in Appendices). This is because PEG crystallizes very rapidly. Indeed, for T_{hold} between 40°C and 10°C, the

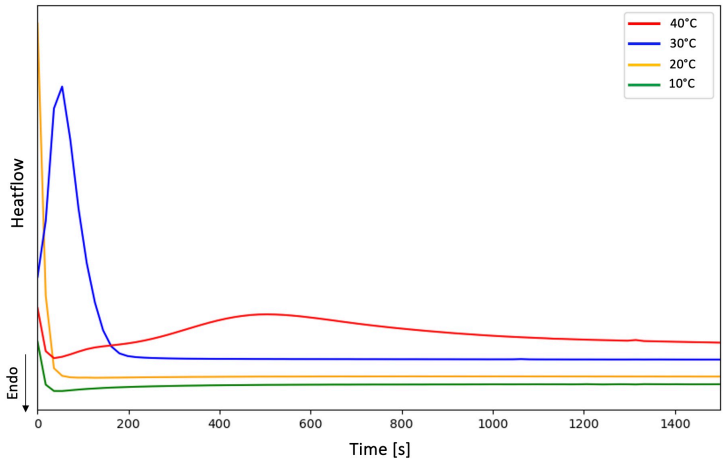

Figure 5.7: Isothermal DSC curves (T_{hold}) of pure PCL between 40°C and 10°C by steps of 10°C (the curves have been shifted vertically for clarity).

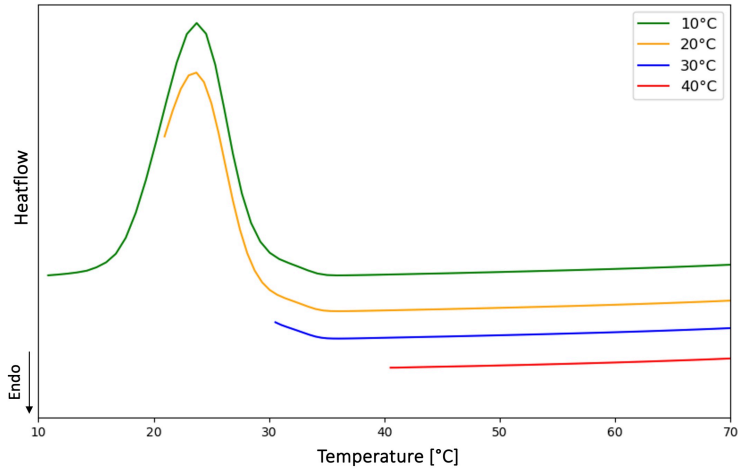

Figure 5.8: DSC curves of the first cooling at -10°C/min before isothermal equilibration between 40°C and 10°C by steps of 10°C for pure PCL (the curves have been shifted vertically for clarity).

crystallization occurred during the first cooling phase before isothermal equilibration. PEG crystallization took place at 44°C, thus before the first isothermal temperature, as shown in Figure 5.9. Therefore, by comparing the DSC results of PEG and PCL, we can conclude that PEG crystallizes more rapidly than PCL, thereby possibly acting as a nucleating agent.

The second behavior represented by the blue curves in Figures 5.3c, d, e, and f exhibits similarities with the first behavior depicted by the red curves. However, a difference is that the melting peaks progressively increase in size as T_{hold} decreases. This trend becomes more evident when examining Figure 5.10, which illustrates the absolute value of the melting enthalpy (ΔH_m) in relation to T_{hold} for the four blends. Examining the behavior of PEG10, PEG20, and PEG30 in Figure 5.10, we observe

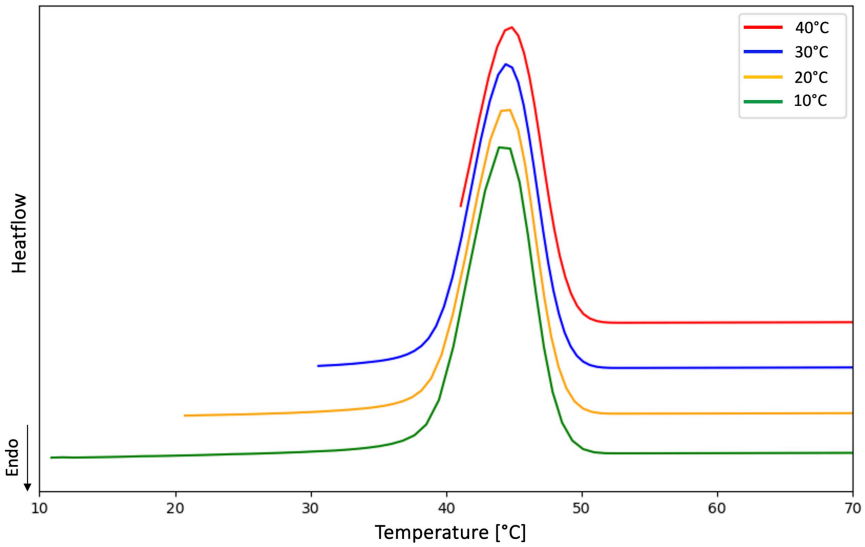

Figure 5.9: DSC curves of the first cooling before isothermal equilibration between 40°C and 10°C by steps of 10°C for pure PEG (the curves have been shifted vertically for clarity).

that ΔH_m remains constant within the temperature range of T_{hold} from 50°C to 40°C. Then, a significant increase in melting enthalpy occurs as T_{hold} decreases from 40°C to 20°C for these three blends. This jump is evidenced by the green highlighting on the curves. This increase justifies the transition from the first to the second behavior within this temperature range. To be more precise, the curve corresponding to T_{hold} of 30°C (the first blue curve in Figure 5.3) clearly marks the transition between the red and blue behavior. This transition curve shows that the transition from one behavior to another occurs progressively, without sudden or abrupt shifts. On the other hand, for PEG50, ΔH_m remains constant from T_{hold} 50°C to 30°C, supporting the choice of the first behavior (red curves) for this blend. Subsequently, the significant increase in ΔH_m occurred between T_{hold} 30°C and 10°C, and it is once again evidenced by the green highlighting on the curves. Thus, the curve corresponding to T_{hold} of 20°C in Figure 5.3 marks the transition between the red and blue behavior for PEG50 blend. Therefore, the result given by Figure 5.10 is consistent with the separation made between the first (red curves) and second (blue curves) behaviors in the different blends.

Following the notable increases in the four curves shown in Figure 5.10, we can observe that ΔH_m remains relatively stable, with a slight maximum peak occurring at T_{hold} -10°C. This temperature represents the point at which the blends exhibit maximal crystallization. Beyond T_{hold} equal to -10°C, ΔH_m gradually decreases as the temperature approaches T_g. Indeed, near T_g, crystallization is less and less favored as molecular movement becomes insufficient.

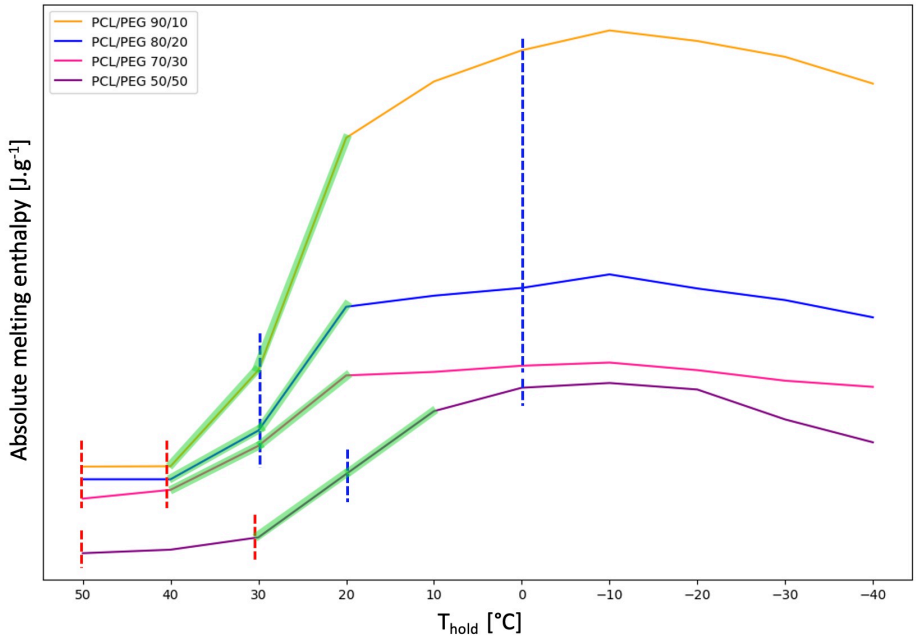

Figure 5.10: Absolute value of the melting enthalpy in function of T_{hold} in the four blends (PEG10, PEG20, PEG30 and PEG50). The green highlight shows the significant jump in enthalpy of melting values between different isothermal temperatures for the different blends. The dotted red and blue lines delineate with their respective colors, the first and second behaviors observed in the fDSC curves.

It is important to specify that fDSC curves are not normalized. fDSC results are qualitative rather than quantitative. This is due to the variations in sample mass between different samples, making it impossible to directly correlate the enthalpy values across curves from different samples. That is why, in Figure 5.10, we haven't compared values between the different curves, but rather compared the trend of the curves.

Now that we have justified the transition from red to blue behavior, we can take a closer look at what happens during the second behavior. As said previously, in this behavior, we can see that the melting peaks progressively increase in size as T_{hold} decreases. However, for PEG10, PEG20 and PEG30 the height of the cold crystallization peak (during heating) remains consistent with that of the upper curves. From this, we deduce that a portion of PCL crystallized during isothermal equilibration, while PEG continued to crystallize during heating. Subsequently, both PCL and PEG crystals melt simultaneously. Then, in the following blue curves, we continue to observe a consistent trend, although there is a notable increase in the quantity of PCL that undergoes crystallization during isothermal equilibration, as indicated by the increase in the melting peak area. Additionally, the width of the melting peak in the final curve of the blue phase expands. In the case of PEG30, two

melting peaks can even be distinguished. Moreover, for this composition, the cold crystallization peak is smaller than in the upper curves, suggesting that a portion of PEG may have begun to crystallize during isothermal equilibration. Verifying this information is challenging because the rapid processes during the isotherm make it difficult to discern multiple crystallization peaks, such as those of PCL and PEG. This difficulty is further compounded by the fact that their transition temperatures are very close. The last curve of the blue behavior in PEG30 can thus be interpreted as a pivotal state between Type II and Type III behavior, with a decrease in PEG cold crystallization and the distinction of two melting peaks, one for PEG and one for PCL. This transition proves that this is a continuous process.

In the case of the blue curves in PEG50, we notice a somewhat different behavior. Indeed, as for the other blends, we can see that the melting peaks progressively increase in size as T_{hold} decreases. However, the height of the cold crystallization peaks decreases significantly compared to the red curves (see blue curves in Figure 5.3f). Thus, for this blend, on the one hand, we have PCL crystallizing during the isotherm. Then, on the other hand, PEG crystallizes both during heating and during the isothermal phase, unlike other blends where PEG crystallizes systematically and only during heating. Finally, as with PEG30 blend, at T_{hold} 0°C (the last blue curve), a second melting peak becomes discernible at lower temperatures.

Furthermore, it is important to mention a notable distinction in behavior between pure PEG and PCL/PEG blends between isothermal temperatures of 30°C and 20°C. To facilitate a comparative analysis of the curves between pure PEG and PCL/PEG blends at these temperatures, we have juxtaposed the curves of pure PEG and the blends for the isothermal temperatures of 30°C and 20°C separately (see Figure 5.11). At T_{hold} of 30°C (Figure 5.11a), we observe cold crystallization of PEG for both pure PEG and blends, highlighted by the dotted black circle. However, at T_{hold} 20°C (Figure 5.11b), we witness a divergence. Indeed, no more cold crystallization of pure PEG is observable, but its melting persists, suggesting crystallization during isothermal equilibration. In contrast, PCL/PEG blends consistently demonstrate cold crystallization of PEG at the isothermal temperature of 20°C, highlighted by the dotted black circle. This is presumably an effect of blending, which persists from T_{hold} 20°C to 0°C. Moreover, it is evident that the crystallization peak during heating corresponds to PEG crystallization for PEG10, PEG20 and PEG30 and to PEG and PCL crystallization for PEG50 as explained previously. This inference is substantiated by the observation that the cold crystallization peak for pure PEG occurs at 29°C, while for PCL/PEG blends (PEG10, PEG20, PEG30, and PEG50), it occurs at 23°C, 25°C, 25°C, and 20°C, respectively, which closely aligns with the cold crystallization temperature of pure PEG.

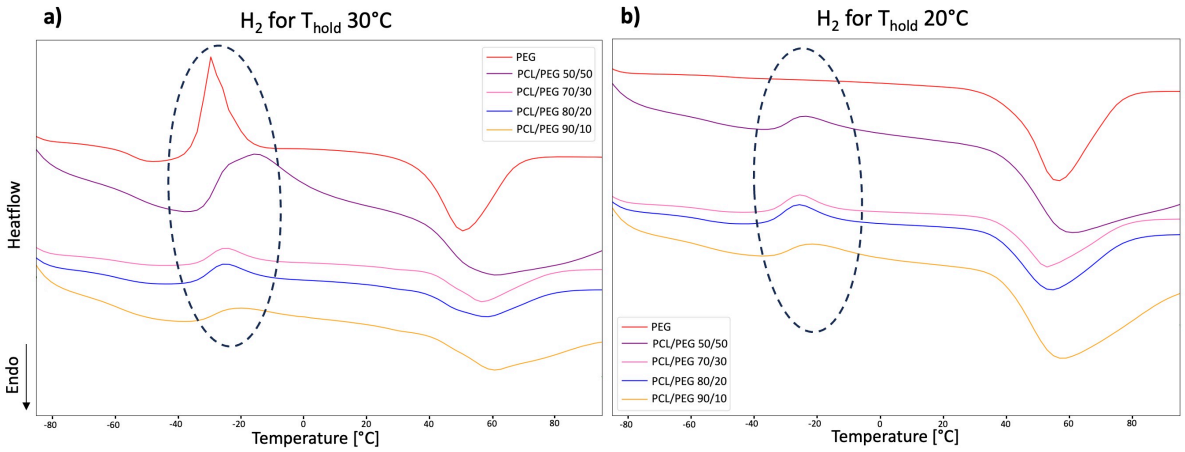

Figure 5.11: fDSC second heating curves (H_2) for the comparison of pure PEG and PCL/PEG blends for T_{hold} at a) 30°C and b) 20°C (the curves have been shifted vertically for clarity). The dotted black circles are visual guides to highlight the difference between graphs a) and b).

Finally, let us examine the final thermal behavior observed across the different blends, represented by the yellow curves in Figure 5.3. These curves represent H_2 for T_{hold} values ranging from -10 to -40°C (from top to bottom). A notable distinction from the previous behavior (blue) is the absence of cold crystallization. Consequently, both PCL and PEG undergo crystallization during isothermal equilibration at T_{hold}. For PEG10 and PEG20 blends, this change results in the splitting of the large melting peak that we could see upon heating at 0°C into two peaks. For PEG30 and PEG50 blends, this splitting was already apparent. As T_{hold} decreases, the two peaks move slightly apart, reinforcing their distinction. Additionally, as T_{hold} decreases, a third "peak" emerges around -20°C. This behavior, previously observed in pure PCL, indicates that this peak, along with the subsequent one, corresponds to the melting of PCL crystals, while the last peak (at higher temperatures) corresponds to the melting of PEG crystals. This deduction was made by comparing the graphs in Figure 5.12, which juxtapose curves of pure PCL, pure PEG, and PCL/PEG blends for T_{hold} -10°C and -40°C. Indeed, we can make an alignment of the melting peak of PEG (red curve) with the last melting peak of the blends, as shown by the dashed black line in Figures 5.12a and b. In addition, we can see the correspondence of the melting peak of pure PCL (green curve) with the first melting peak of the blends for T_{hold} -10°C and -20°C, highlighted by the first dotted black line in Figure 5.12a, and the first two melting peaks of the blends for T_{hold} -30°C and -40°C, highlighted by the first and second dotted black lines in Figure 5.12b.

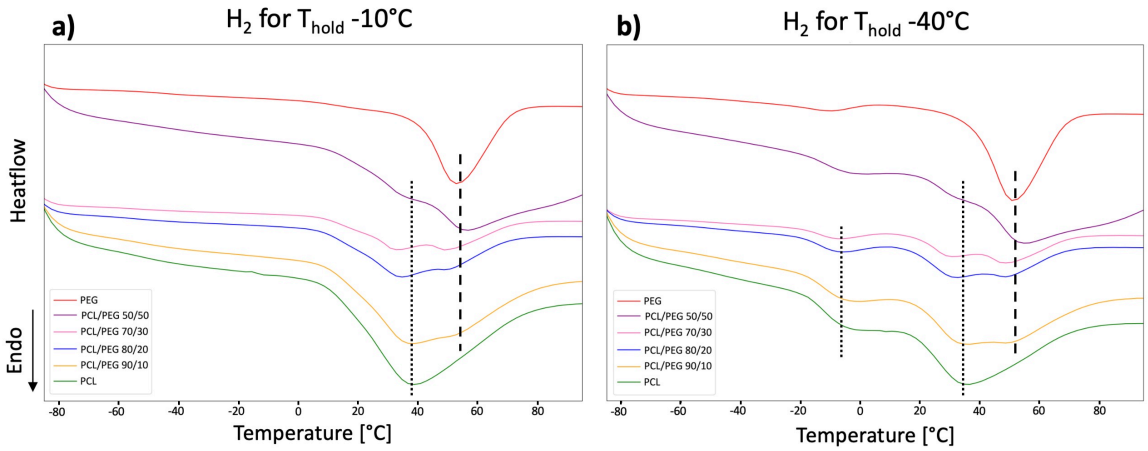

Figure 5.12: fDSC second heating curves (H_2) for the comparison of pure PCL, pure PEG and PCL/PEG blends for T_{hold} at a) -10°C and b) -40°C (the curves have been shifted vertically for clarity). The dotted and dashed black lines are visual guides to see the alignment of the different melting peaks between pure PCL, pure PEG and the different blends.

Therefore, from these observations, it appears that neither the melting of PCL nor PEG is significantly affected by their blending, suggesting considerable phase separation; however, under certain conditions, there is still some influence of PEG on PCL and vice versa, which does not rule out the existence of partial miscibility.

5.2 Phase separation

Summing up, three different types of behavior can be distinguished depending on equilibration temperatures (Figure 5.3). For Type I behavior (red curves), only PEG crystallizes from PEG-rich regions created by a liquid-liquid phase separation process in the amorphous blend. PCL does not crystallize.

For Type II (blue curves), both PCL and PEG crystallize. PCL crystallizes during isothermal equilibration, whereas PEG crystallizes during heating. We can also identify a single melting point for PCL and PEG. Type II behavior thus indicates either a liquid-liquid phase separation from a non-homogeneous blend or a liquid-solid phase separation from a homogeneous blend. Assuming a liquid-liquid phase separation, we initially would have two distinct phases in the liquid state due to the immiscibility of the two polymers. During isothermal equilibration, PCL would crystallize first in its own domain. Upon quenching and subsequent heating of the sample, PEG, which has not yet crystallized, would then undergo crystallization. By the end of this process, each polymer would have crystallized in its own environment, unaffected by the presence of the other polymer. Thus, PEG would crystallize as pure PEG and PCL as pure PCL. However, at this stage, the second hypothesis of a liquid-solid phase separation must also be considered. In this scenario, the two polymers are miscible and form a uniform blend. PCL starts to crystallize first, which forces PEG out of the crystallizing PCL region. This results in the accumulation of PEG, forming PEG-enriched elongated regions either between spherulites or within fibrils. Here, it is the crystallization process that induces phase separation. Between these two scenarios, the underlying mechanisms differ fundamentally. Liquid-liquid phase separation is driven by the immiscibility of the two polymers, while liquid-solid phase separation is driven by the crystallization process. Further experiments, particularly morphological studies, are needed to determine which hypothesis is correct. However, examining the fDSC curves for the different blends in Figure 5.3 suggests that the signals appear to be a superposition of pure PCL and pure PEG signals. This observation supports the hypothesis of liquid-liquid phase separation, where PEG-rich and PCL-rich regions exist with minimal interaction between the two polymers. If liquid-solid separation were occurring, we would expect the crystallization kinetics of the polymer blends to be significantly more disrupted.

Finally, Type III behavior (yellow curves), where both PCL and PEG crystallize during isothermal equilibration (according to Figure 7.1 in the Appendices), indicates either liquid-liquid or liquid-solid phase separation. The presence of a single crystallization peak during isothermal equilibration suggests the simultaneous crystallization of PCL and PEG. However, as discussed earlier, the limitations of fDSC may obscure certain

phenomena during this process. Therefore, to better understand these dynamics, DSC measurements were conducted, as shown previously, to observe the behavior before and during the isothermal equilibration of pure PCL and pure PEG. These measurements revealed that PEG crystallizes more quickly than PCL, and therefore that PEG crystallizes first. Under the liquid-liquid phase separation hypothesis, this would result in a scenario similar to Type II behavior. In contrast, if liquid-solid phase separation was occurring, PEG would begin to crystallize first, forming relatively large spherulites within a continuous PCL phase. PEG would thus coexist with PCL chains of varying viscosity, followed by PCL crystallizing around the PEG spherulites, entrapping them. This would significantly affect the blend's kinetics. However, the fDSC curves for blends do not show significant changes compared to those of the pure compounds, making the liquid-liquid separation hypothesis more plausible.

5.3 Morphology of polymer blends

5.3.1 Surface analysis of polymer blends

Subsequently, the analyses focus on the study of the molecular structure and the spatial organization of polymer chains through polarized optical microscopy (POM) and scanning electron microscopy (SEM) analysis, conducted before and after the selective removal of PEG. Pores or cavities then result from the local elimination of PEG. This approach elucidates PEG location within the blend across various scales and can be related to the previously established phase diagram.

Uncrystallized films

We therefore started by examining POM images of PCL/PEG films with concentrations of 95/5, 85/15 and 80/20 after solvent evaporation. It appears that the evaporation process misled us about the porosity of the mixture, as holes formed due to the evaporation of the solvent. Nevertheless, intriguing images were observed with POM before (Figure 5.13 a, b and c) and after PEG extraction (Figure 5.13 d, e and f). Specifically, PCL spherulites were visible, and after PEG extraction, new black dots appeared. The increase in the number of black dots with increasing PEG concentration in the mixture suggests that these are holes that have been filled by PEG prior to extraction.

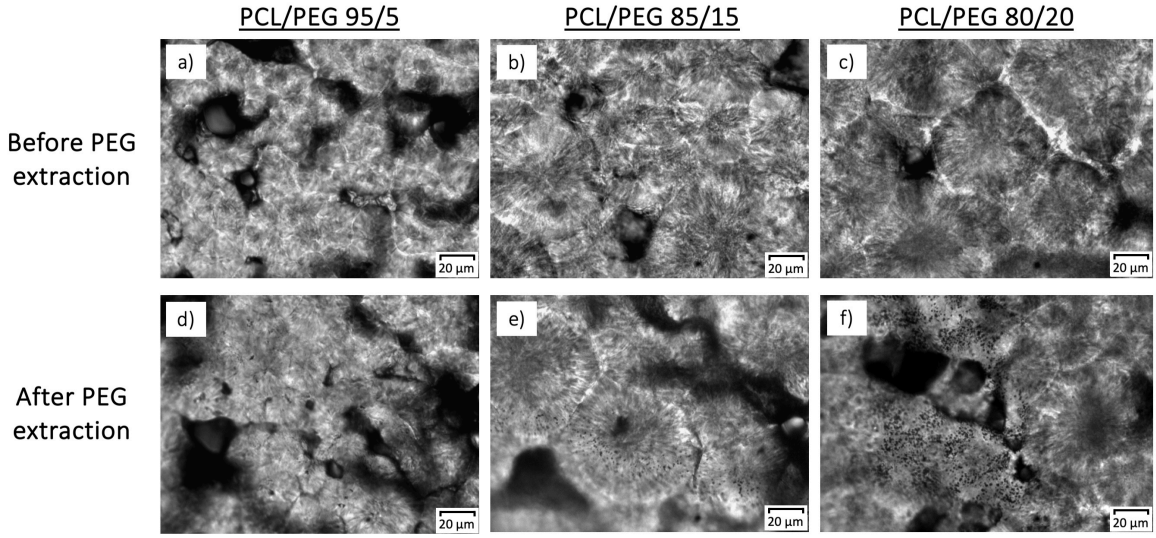

Figure 5.13: POM images of PCL/PEG blends after solvant evaporation a) 95/5, b) 85/15 and c) 80/20 before PEG extraction and d) 95/5, e) 85/15 and f) 80/20 after PEG extraction (magnification x50).

Then, for a more detailed examination, we used SEM. Consistent with our earlier observations, solvent evaporation affected the surface of the samples. However, an interesting image was found for PEG20, revealing PCL spherulites with PEG interspersed between them, as shown in Figure 5.14. The holes in the PCL regions are attributed to solvent evaporation, as previously mentioned. We also examined images after PEG extraction. However, the results were inconclusive, as it was challenging to distinguish between pores caused by solvent evaporation and those resulting from PEG extraction.

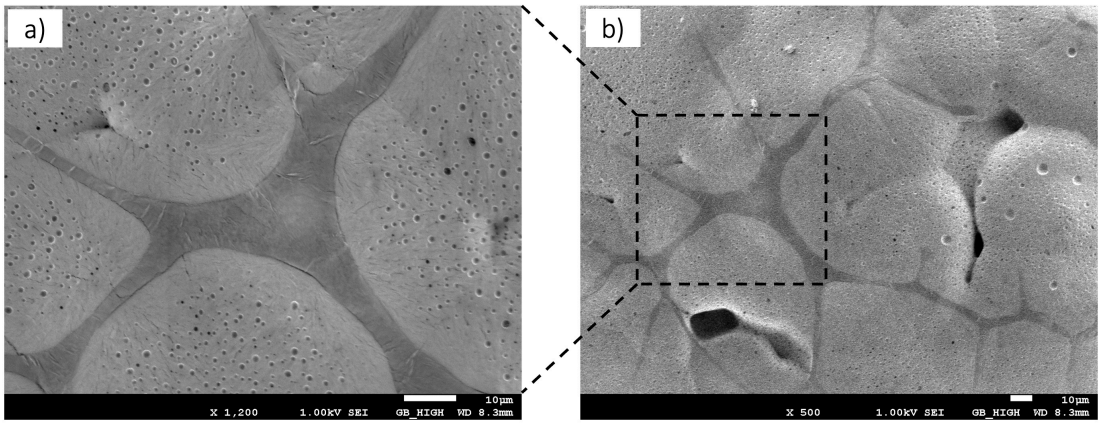

Figure 5.14: SEM images of PCL/PEG 80/20 film after solvant evaporation. a) magnification x1200 and b) overall view (magnification x500). PCL is represented in light gray and PEG in darker gray.

PEG extraction

Then, as we also work on films after PEG extraction, it is interesting to know whether the extraction method was able to extract all the PEG contained in the films or not. In fact, we observed that not all PEG was extracted after extraction. Indeed, the weights before and after extraction do not exactly match the percentage of PEG that had to be extracted. In Table 5.2, the numbers in red represent the percentage of PEG in the mixture, and in the case of the PCL/PEG/Aspirin mixture, they represent the percentages of both PEG and aspirin. If all the PEG had been extracted after soaking the samples in water for 24 hours, the numbers in red would match the numbers in the right-hand column, which indicates the percentage of mass lost. However, these measurements are somewhat rough because we weigh relatively small samples on a balance, so the results should be interpreted with caution. Nonetheless, we observe that as the proportion of PEG in the mixture increases, the weight loss value increasingly approximates the initial proportion of PEG in the mixture. With this information, we can hypothesize about the structure of the mixture. For example, in the case of PEG5 blend, there is not much PEG,

suggesting that PEG is well-distributed within the PCL. PEG dissolves in the amorphous phase of PCL, making it difficult to extract, which is why the 5% of PEG is barely extracted. Thus, we might think that, initially, PEG is mainly located within the PCL spherulits. However, if more PEG is added, the PCL spherulits can become saturated with PEG, causing excess PEG to accumulate outside or between the PCL spherulits. The PEG located between the spherulits would be more easily extracted than the PEG trapped in the PCL spherulits, which would explain why the higher the proportion of PEG in the mixture, the more it is extracted.

Blends composition	**Weight loss (%)**
Uncrystallized 95/5	1
Uncrystallized 90/10	2.5
Uncrystallized 85/15	7
Uncrystallized 80/20	12
Uncrystallized 70/30	23
Uncrystallized 50/50	50
Crystallized 95/5	2
Crystallized 90/10	5
Crystallized 85/15	8
Crystallized 80/20	14
Crystallized 70/30	22
Crystallized 50/50	48
Crystallized PCL/PEG/Asp 60/20/20	33.5

Table 5.2: Weight loss after PEG extraction in PCL/PEG films after solvent evaporation and after crystallization for different PEG concentrations. The numbers in red represent the percentage of PEG in the mixture and in the case of the PCL/PEG/Asp mixture, they represent the percentage of PEG and aspirin.

Crystallized films

For the subsequent analysis, we decided to work with crystallized films in order to avoid the problem of holes caused by solvent evaporation and to guarantee a better thermally equilibrated structure. To achieve this, PCL/PEG blends of various compositions were melted and rapidly cooled to room temperature (approximately 25°C). Subsequently, PEG was extracted using distilled water, and the porous films were allowed to air dry at room temperature for 24 hours prior to analysis. To assess the influence of composition on the resulting sample morphology, the surface of the films was examined using SEM (Figure 5.15, depicting PEG5, PEG10, PEG15, PEG20 and PEG30).

Surface observations of the various blends provided further insights into their morphology, particularly regarding the distribution of PEG. Indeed, the surface concentration of PEG appears to increase from PEG5 to PEG15, with the surface becoming progressively rougher. However, beyond this concentration, for PEG20 and PEG30, the PEG surface concentration seems to decrease slightly. This change in surface morphology is not reflected in the fDSC curves, indicating it may be a surface phenomenon. To verify this hypothesis, it would be necessary to examine the structure in the thickness of the samples. Furthermore, for PCL/PEG blends in Figure 5.15, regions rich in pure PEG are observed on the surface. This observation is consistent with the fDSC data, indicating limited miscibility and reminding us more of a liquid-liquid phase separation, illustrated in Figure 5.16, rather than liquid-solid phase separation. Indeed, if liquid-solid phase separation were occurring, we would observe crystallization with the second component being expelled into the spherulitic structure. This would result in the formation of channels of the second component between packets of lamellae of the first component, which is not evident here. To verify this, we need to examine films crystallized at different temperatures, as our current observations are limited to crystallization at 25°C.

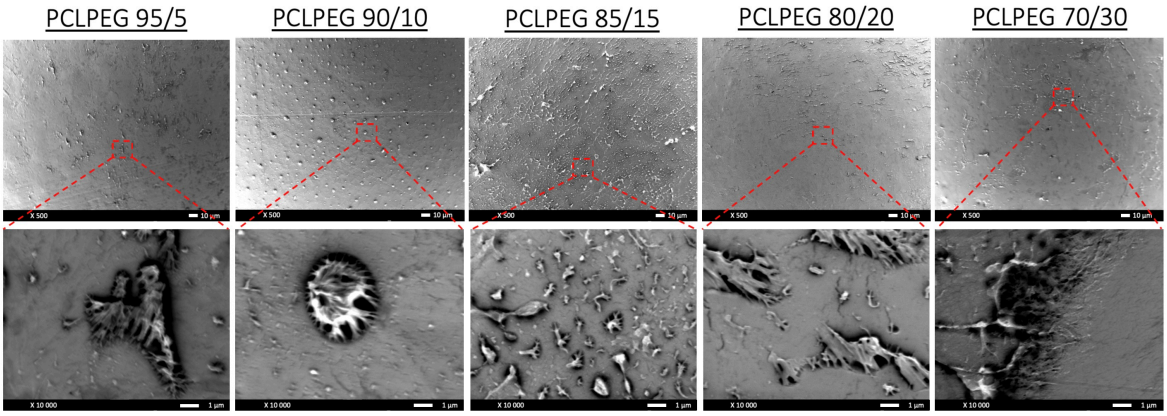

Figure 5.15: PCL/PEG blends of compositions 95/5, 90/10, 85/15, 80/20 and 70/30 with magnification of x500 (first line) and x10 000 (second line) before PEG extraction.

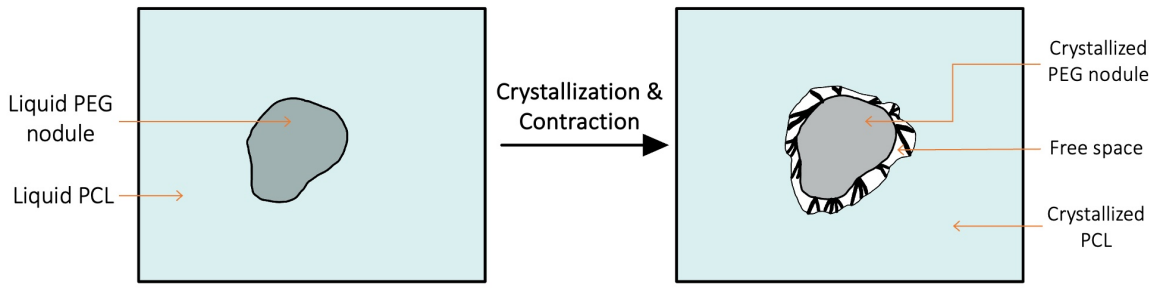

Figure 5.16: Illustration of liquid-liquid phase separation in PCL/PEG blends before and after PEG crystallization and contraction.

The next step is to analyze the images after PEG extraction, realized by immersing the various samples in water (see Figure 5.17). These images confirm that the elements observed on the surface prior to PEG extraction were PEG. Indeed, in PEG15 and PEG20, cavities have now formed in the areas where PEG was previously located. Moreover, the images described in figure 5.17 closely resemble those obtained with POM (see figure 5.13), where cavities were represented by black points. However, these cavities do not appear to be interconnected and do not form a continuous network. As previously mentioned, it is essential to examine in the sample thickness to determine if this behavior is consistent throughout the sample.

Finally, the PEG50 crystallized film was contaminated. Thus, we were enable to obtain any results from this sample.

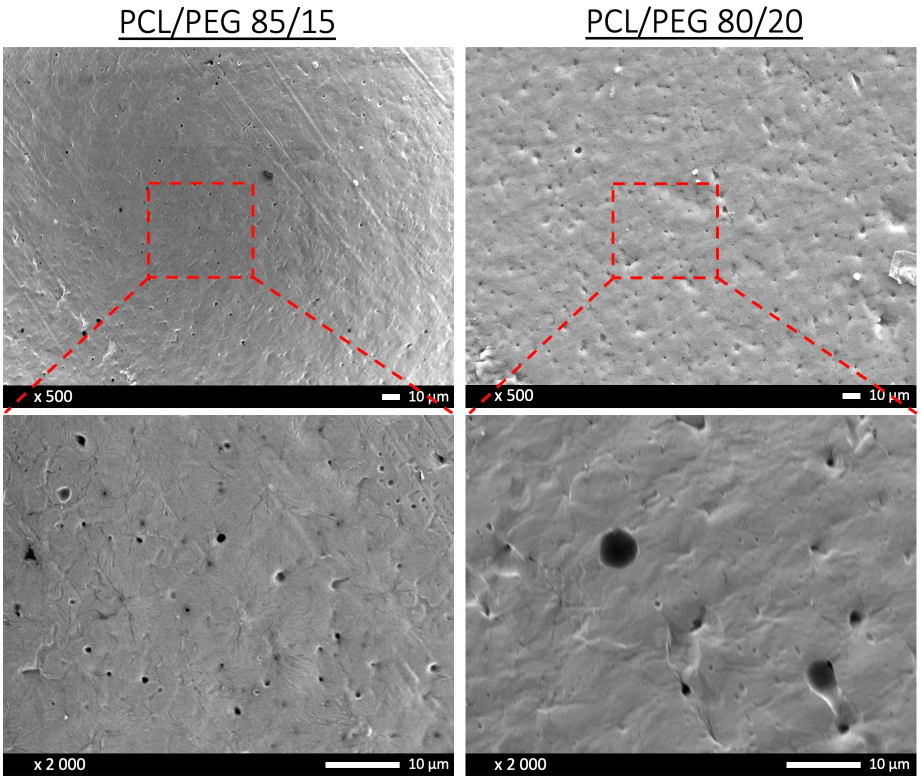

Figure 5.17: PCL/PEG blends of compositions 85/15 and 80/20 with magnification of x500 and x2 000 after PEG extraction.

5.3.2 Spectroscopic analysis of polymer blend films

In this section, we complete our study of polymer blend morphology using a spectroscopic approach. The use of FTIR enriches our previous analyses carried out by SEM. By combining these two techniques, we gain an in-depth understanding of the molecular composition and distribution of components within these polymeric films.

To start, we needed to identify the specific peaks characteristic of PCL and PEG. These peaks are the ones that exhibit significant prominence for one component while being absent in the other. This step is crucial in order to be able to detect any changes that occur when the two components are mixed together. Thus, we found the peak at 1723 cm^{-1} for PCL and 1104 cm^{-1} for PEG, as shown in Figure 5.18.

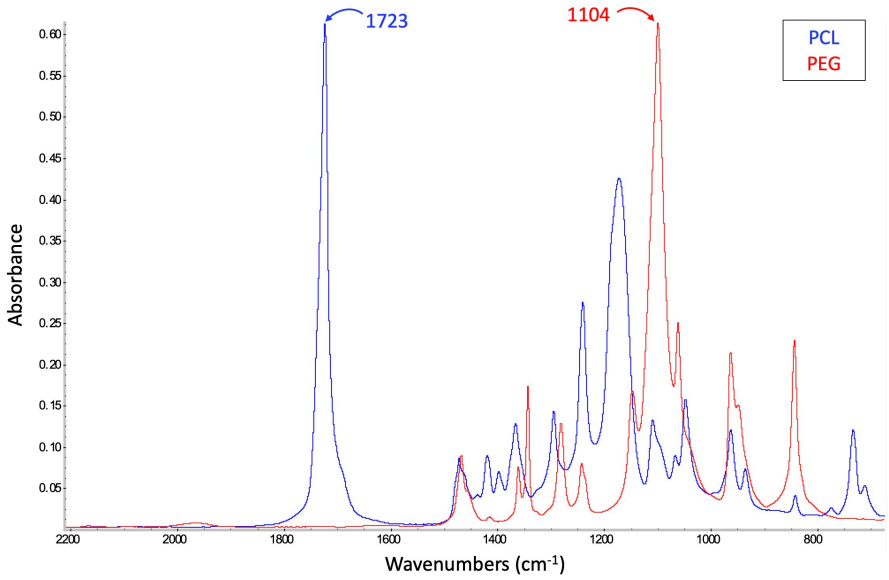

Figure 5.18: FTIR spectrum of pure PCL and pure PEG.

Then, in order to obtain interpretable values for subsequent analysis, we opted to establish a correlation between absorbance values and the concentration of PEG in PCL/PEG films. To achieve this, we conducted experiments using films containing varying concentrations of PEG. Three points were selected from non-crystallized films to ensure that they represented the most homogeneous areas possible, thereby being indicative of the compositions of PEG5, PEG10, PEG15, PEG20, PEG30 and PEG50 samples. Subsequently, the heights of characteristic peaks corresponding to PEG and PCL were measured for each of the three points. The absorbance values for PEG were divided by those of PCL, and the average of the three points was calculated. The resulting correlation is shown in Figure 5.19. The linear regression curve was then added to establish the linear relationship between the absorbance values and PEG concentrations.

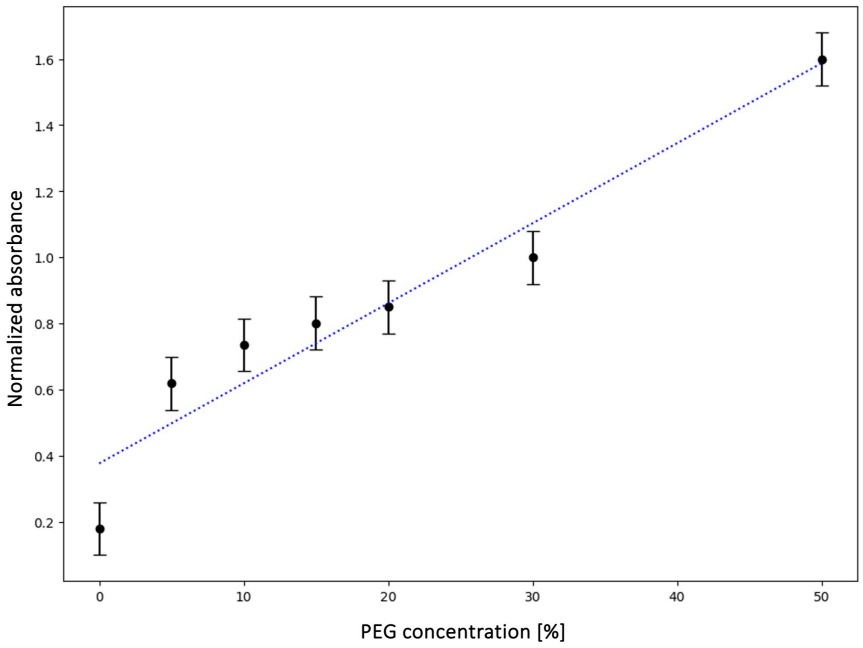

Figure 5.19: Correlation between normalized absorbance values and PEG concentrations. The dotted blue line represents the linear regression of the black points. Error bars indicate the standard error for each point, as each point was calculated from the mean of three measurements.

Then, with the absorption-PEG concentration graph established, our focus naturally shifts towards FTIR mapping analysis. Indeed, FTIR mapping provides valuable insights into the homogeneity and spatial distribution of these polymers in the film matrix. However, a challenge arises in correlating FTIR mapping data with SEM imaging due to the differing depths of analysis; while SEM provides surface-level insights, FTIR mapping delves deeper. Moreover, the lateral resolution between SEM and FTIR is also very different, with FTIR achieving approximately 10 μm while SEM reaches approximately 10 nm. We can therefore expect differences in results between the two techniques. Nevertheless, despite this disparity, noteworthy similarities can still be observed between the FTIR mapping (Figure 5.20) result and the SEM image (Figure 5.15) of PEG20 crystallized films. Indeed, in the FTIR mapping, yellow areas indicate higher concentrations of PEG compared to green areas. This further supports the assertion that the observed roughness in the SEM images corresponds to PEG. However, upon analyzing the absorbance scale and overlaying it onto our graph, we observe a 20% PEG content in the yellow zones, traditionally associated with pure PEG zones. This difference can be attributed to the fact that PEG spherulites are certainly not entirely pure and also to the limited resolution of FTIR, which mixes the signal.

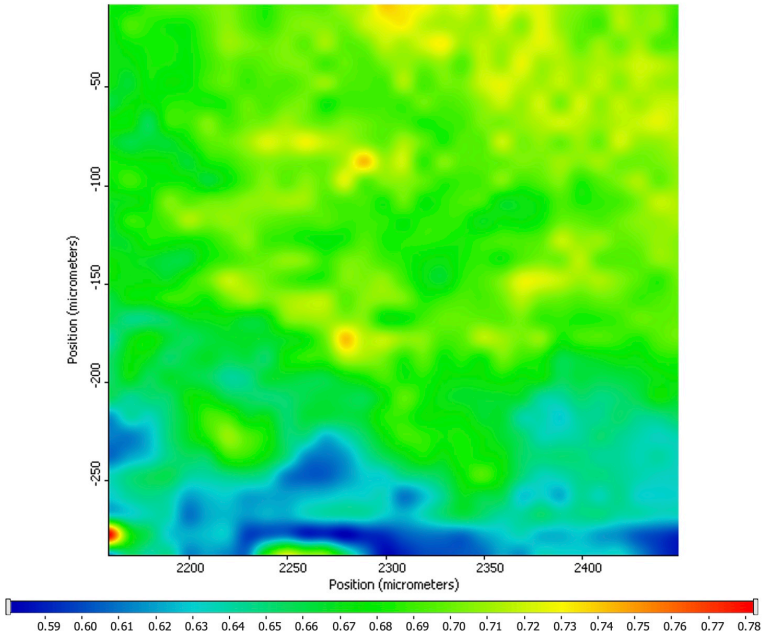

Figure 5.20: Mapping of PEG20 film after crystallization. On the scale bar, blue indicates a lower PEG concentration, and red indicates a higher PEG concentration.

5.4 Blending with Aspirin

This section will delve into a brief analysis of the effects arising from the integration of a third component into our binary mixture of PCL and PEG. This supplementary component, aspirin, assumes the pivotal role of the active pharmaceutical ingredient. Indeed, a key aim of this research is to explore whether the incorporation of an API in this binary mixture may yield enhancements in the sustained release profile of the active ingredient within the physiological milieu.

Our analysis will be based on the analysis of SEM images of a blend consisting of 60% PCL, 20% PEG, and 20% aspirin (Asp20). Images 5.21 a, b, c, and d showcase the crystallized film of Asp20 blend, whereas images 5.21 e, f, g, and h depict the crystallized film of the same blend following the extraction of PEG and aspirin.

In image (a), the distinct white formations represent the aspirin crystals. These crystals are clearly identifiable and indicate that aspirin is not miscible within the PCL/PEG matrix, instead forming separate crystalline structures. Then, in image (b), which represents a magnification of image (a), we can see what appear to be holes. However, upon closer examination at higher magnifications, such as in images (c), it becomes evident that these features are more accurately described as bumps rather than holes. These bumps exhibit a texture and pattern consistent with the characteristics observed in previous studies of PCL/PEG blends (see Figure 5.15). Finally, in images (e) to (h), where aspirin crystals and PEG have been extracted, aspirin is no longer visible and numerous holes have appeared. These holes are likely created by the PEG component. Nonetheless, the abundance of these holes suggests that aspirin may also play a significant role in their formation.

The overall analysis reveals that the presence of aspirin in the PCL/PEG blend, as well as the matrix after the extraction of aspirin and PEG, does not exhibit any specific interactions within the matrix. This suggests that this ternary mixture may not significantly enhance the release of aspirin in the body. However, further investigation could prove beneficial. One potential avenue for future research is to first create a binary blend, extract the PEG and then introduce aspirin to determine if it localizes within the PEG-created voids. Nonetheless, it is important to note that the observed PEG holes do not form continuous networks, raising questions about the effectiveness of this approach. As previously mentioned, our observations are limited to the surface characteristics; the internal structure of the material could present different interactions and behaviors.

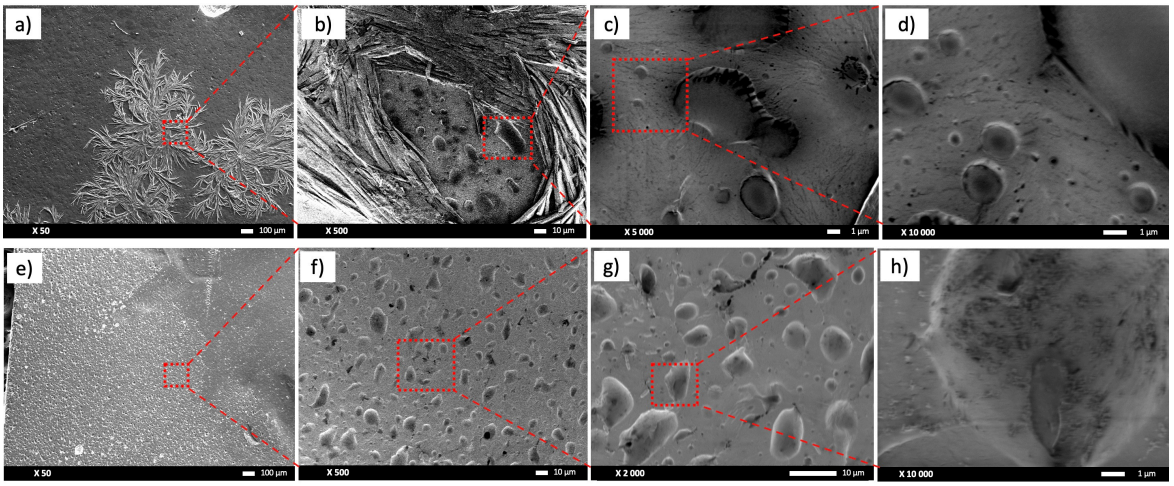

Figure 5.21: SEM images of PCL/PEG/aspirin blend before (a, b, c and d) and after (e, f, g and h) PEG and aspirin extraction with magnification of x50 (a and e), x500 (b and f), x2000 (g), x5000 (c) and x10 000 (d and h).

In conclusion, while initial findings indicate limited promise for this ternary mixture in enhancing aspirin release, a more in-depth examination, particularly of the internal material structure, could be done to fully understand the potential of this system.

Chapter 6

Conclusions

In conclusion, this thesis has thoroughly explored the thermal and structural properties of PCL/PEG blends with different concentrations of PEG for the purpose of developing 3D-printable drugs. The primary aim was to investigate the interactions and phase separations between PCL and PEG and to assess whether the inclusion of PEG could enhance the release profile of aspirin within the blend. The research involved extensive thermal and morphological analysis of the PCL/PEG blends, examining their behavior at various ratios and temperatures to identify optimal conditions.

The main results of this study focus on the thermal behavior of PCL/PEG blends. The fDSC analysis revealed that PCL and PEG exhibit distinct thermal behaviors with very similar transition temperatures, such as glass transition and melting temperatures. A critical observation from the fDSC curves is that the blends show superimposed thermal curves of the individual polymers. This suggests a phase separation rather than a homogeneous mixture and therefore limited miscibility between PCL and PEG. In addition, the fDSC results indicated that the expected plasticizing effect of PEG was not significant. Indeed, faster crystallization rates would typically indicate a plasticizing effect, but no substantial difference was observed with or without PEG, except for an additional PEG melting peak.

In the subsequent step of our study, we took a closer look at the phase separation and morphological analysis of the blends. Using fDSC curves of PCL/PEG blends, we highlighted three distinct behaviors of the mixtures. The first type of behavior was seen for temperatures above 40°C (red curves). During this phase, only PEG crystallized during heating, resulting in a liquid-liquid phase separation. Then, between 30°C and 0°C (blue curves), type II behavior appeared, characterized by the crystallization of both PCL and PEG during isothermal equilibration and heating, respectively. This phenomenon led to the formulation of two hypotheses: either a liquid-liquid phase separation or a liquid-solid phase separation. Our results

leaned towards supporting the idea of liquid-liquid separation. Furthermore, between -10°C and -40°C (yellow curves), a type III behavior emerged, where both PCL and PEG crystallized during isothermal equilibration but PEG crystallized before PCL. Once again, liquid-liquid and liquid-solid phase separation could be considered, but liquid-liquid separation is more likely, according to our results. Upon analysis, it becomes evident that the concentration of PEG does not exert a significant influence on the miscibility and phase separation tendencies of PCL/PEG blends.

Afterwards, SEM images revealed the immiscibility of PCL and PEG, highlighting the tendency of PEG to separate from PCL, forming distinct phases. In addition, after PEG extraction, the presence of isolated porosities in the mixture became evident. However, these porosities did not appear to be interconnected, raising questions about their effectiveness in enhancing aspirin release.

Finally, according to our work, the addition of aspirin to the PCL/PEG matrix showed no real advantage for aspirin release. Aspirin gave rise to the formation of a separated crystalline phase, restricting its interaction with the polymer matrix and not favoring a sustained release mechanism.

Looking forward, future research could be focused on extrusion techniques to potentially influence phase separation and improve the distribution of PEG in the matrix, thus obtaining a more homogeneous blend with enhanced drug release properties. Additionally, the study of film thickness could help determine whether the effects observed are surface-related or pervasive throughout the material.

Overall, this thesis has contributed to the growing body of knowledge on biodegradable polymers in biomedical applications, specifically in the context of developing 3D printable drugs. While the current ternary system of PCL/PEG/aspirin showed limited promise in enhancing drug release, the findings provide a valuable foundation for future research aimed at improving the efficacy and precision of personalized medicine through advanced 3D printing technologies. Future work could focus on modifying one of the two polymers in order to find a better blend that would achieve better miscibility and controlled drug release profiles.

Bibliography

[1] Personalised medicine - European Commission, **2024**, https://health.ec.europa.eu/medicinal-products/personalised-medicine_en.

[2] Personalized Medicine, https://www.genome.gov/genetics-glossary/Personalized-Medicine.

[3] V. M. Vaz, L. Kumar, *AAPS PharmSciTech* **2021**, *22*, 49.

[4] L. Lu, A. G. Mikos, *MRS Bulletin* **1996**, *21*, 28–32.

[5] E. Malikmammadov, T. E. Tanir, A. Kiziltay, V. Hasirci, N. Hasirci, *Journal of Biomaterials Science Polymer Edition* **2018**, *29*, 863–893.

[6] F. Koch, O. Thaden, S. Conrad, K. Tröndle, G. Finkenzeller, R. Zengerle, S. Kartmann, S. Zimmermann, P. Koltay, *Journal of the Mechanical Behavior of Biomedical Materials* **2022**, *130*, 105–219.

[7] M.-O. Christen, F. Vercesi, *Clinical Cosmetic and Investigational Dermatology* **2020**, *13*, 31–48.

[8] What is polycaprolactone? Structure, Density, and Applications, EuroPlas, https://europlas.com.vn/en-US/blog-1/what-is-polycaprolactone-structure-density-and-applications.

[9] M. V. Deshpande, A. Girase, M. W. King, *Polymers* **2023**, *15*, 3819.

[10] Y. Hu, Y. Liao, Y. Zheng, K. Ikeda, R. Okabe, R. Wu, R. Ozaki, J. Xu, Q. Xu, *Polymers* **2022**, *14*, 3646.

[11] J.-M. Haudin, S. Boyer, *International Polymer Processing* **2017**, *32*, 545–554.

[12] Amorphous vs. Crystalline Polymers | PCI Magazine, https://www.pcimag.com/articles/111547-amorphous-vs-crystalline-polymers.

[13] M. Arif P, N. Kalarikkal, S. Thomas **in***Crystallization in Multiphase Polymer Systems* **2017**, **pages** 1–16.

[14] L. McKeen **in***The Effect of Long Term Thermal Exposure on Plastics and Elastomers* (**editor**: L. McKeen), Plastics Design Library, William Andrew Publishing, **2021**, **chapter** 11, **pages** 313–332.

[15] L. Jiang, J. Zhang **in***Handbook of Biopolymers and Biodegradable Plastics* (**editor**: S. Ebnesajjad), Plastics Design Library, William Andrew Publishing, Boston, **2013**, **chapter** 6, **pages** 109–128.

[16] M.-T. I. I. all rights reserved, Détermination de la cristallisation des polymères par analyse thermique, **2023**.

[17] Crystallization and recrystallization of polymers » LINSEIS, https://www.linseis.com/en/wiki-en/crystallization-and-recrystallization-of-polymers/.

[18] A. Toda **in***Encyclopedia of Polymers and Composites* (**editor**: S. Palsule), Springer Berlin Heidelberg, Berlin, Heidelberg, **2021**, **pages** 1–12.

[19] N. Nurazzi, M. Norrrahim, S. Shazleen, M. Harussani, F. Sabaruddin, M. Asyraf **in***Polymer Crystallization* John Wiley & Sons, Ltd, **2023**, **pages** 1–12.

[20] A. Fernández-Tena, R. A. Pérez-Camargo, O. Coulembier, L. Sangroniz, N. Aranburu, G. Guerrica-Echevarria, G. Liu, D. Wang, D. Cavallo, A. J. Müller, *Macromolecules* **2023**, *56*, 4602–4620.

[21] P. A. Klonos, N. D. Bikiaris, E. Christodoulou, A. Zamboulis, G. Z. Papageorgiou, A. Kyritsis, *Polymer* **2022**, *242*, 124603.

[22] M. Zabihzadeh Khajavi, A. Ebrahimi, M. Yousefi, S. Ahmadi, M. Farhoodi, A. Mirza Alizadeh, M. Taslikh, *Food Engineering Reviews* **2020**, *12*, 346–363.

[23] C. J. Kuo, W. L. Lan **in***Advances in Filament Yarn Spinning of Textiles and Polymers* (**editor**: D. Zhang), Woodhead Publishing, **2014**, **pages** 100–112.

[24] I. Castilla-Cortázar, A. Vidaurre, B. Marí, A. J. Campillo-Fernández, *Polymers* **2019**, *11*, 1099.

[25] D. R. Rohindra, J. R. Khurma, *The South Pacific Journal of Natural and Applied Sciences* **2008**, *25*, 53–60.

[26] V. Speranza, A. Sorrentino, F. De Santis, R. Pantani, *The Scientific World Journal* **2014**, *2014*, 1–9.

[27] L. S. O. Pires, M. H. F. V. Fernandes, J. M. M. de Oliveira, *Journal of Thermal Analysis and Calorimetry* **2018**, *134*, 2115–2125.

[28] M. Schulz, A. Seidlitz, A. Petzold, T. Thurn-Albrecht, *Polymer* **2020**, *196*, 122441.

[29] M. Bartnikowski, T. R. Dargaville, S. Ivanovski, D. W. Hutmacher, *Progress in Polymer Science* **2019**, *96*, 1–20.

[30] I. Castilla-Cortázar, J. Más-Estellés, J. M. Meseguer-Dueñas, J. L. Escobar Ivirico, B. Marí, A. Vidaurre, *Polymer Degradation and Stability* **2012**, *97*, 1241–1248.

[31] T. K. Dash, V. B. Konkimalla, *Journal of Controlled Release: Official Journal of the Controlled Release Society* **2012**, *158*, 15–33.

[32] N. Alharbi, A. Daraei, H. Lee, M. Guthold, *Materials Today Communications* **2023**, *35*, 105773.

[33] A. Liaskoni, R. D. Wildman, C. J. Roberts, *International Journal of Pharmaceutics* **2021**, *597*, 120330.

[34] **in** *Wikipedia* **2024**.

[35] R. E. Cameron, A. Kamvari-Moghaddam **in** *Durability and Reliability of Medical Polymers* (**editors**: M. Jenkins, A. Stamboulis), Woodhead Publishing, **2012**, **chapter** 5, **pages** 96–118.

[36] P. Nguyen Tri, R. E. Prud'homme, *Macromolecules* **2018**, *51*, 7266–7273.

[37] S. Moore, What is Polyethylene Glycol (PEG)?, News-Medical, **2020**, https://www.news-medical.net/life-sciences/What-is-Polyethylene-Glycol-(PEG).aspx.

[38] Polyethylene glycol, https://www.chemeurope.com/en/encyclopedia/Polyethylene_glycol.html.

[39] Polyethylene glycol 6000 for synthesis, http://www.sigmaaldrich.com/.

[40] J. Herzberger, K. Niederer, H. Pohlit, J. Seiwert, M. Worm, F. R. Wurm, H. Frey, *Chemical Reviews* **2016**, *116*, 2170–2243.

[41] Important Properties of Polyethylene Glycols which make Them Important Products for Pharmaceutical Applications, https://www.rimpro-india.com/articles1/important-properties-of-polyethylene-glycols-which-make-them-important-products-for-pharmaceutical-applications.html.

[42] A. A. D'souza, R. Shegokar, *Expert Opinion on Drug Delivery* **2016**, *13*, 1257–1275.

[43] D. Q. M. Craig, *Thermochimica Acta* **1995**, *248*, 189–203.

[44] W.-T. Chuang, K.-S. Shih, P.-D. Hong, *Journal of Polymer Research* **2005**, *12*, 197–204.

[45] M. Guastaferro, L. Baldino, S. Cardea, E. Reverchon, *The Journal of Supercritical Fluids* **2022**, *186*, 105611.

[46] C. Luo, W. Chen, Y. Gao, *Polymer Science Series A* **2016**, *58*, 196–205.

[47] W.-T. Chuang, U.-S. Jeng, H.-S. Sheu, P.-D. Hong, *Macromolecular Research* **2006**, *14*, 45–51.

[48] Aspirin Formula: Properties, Chemical Structure and Uses, Extramarks, https://www.extramarks.com/studymaterials/formulas/aspirin-formula/.

[49] S. Catherine, *Journal of Clinical & Experimental Pharmacology* **2021**, *11*, 164.

[50] C. Fossum, Synthesis of Aspirin, **2012**.

[51] Wikipedia, Aspirin, **2024**.

[52] Aspirin Formula: Structure, Preparations and Properties, https://www.toppr.com/guides/chemistry-formulas/aspirin-formula/.

[53] Unacademy, The Properties of Aspirin, **2022**.

[54] Science blog: Making aspirin crystals. — Steemit, https://steemit.com/zzan/@josalarcon2/science-blog-making-aspirin-crystals.

[55] Wikipedia, Salicylate poisoning, **2023**.

[56] NHS England » Personalised medicine, https://www.england.nhs.uk/healthcare-science/personalisedmedicine/.

[57] D. Stefanicka-Wojtas, D. Kurpas, *Journal of Personalized Medicine* **2023**, *13*, 380.

[58] A. A. Alqahtani, M. M. Ahmed, A. A. Mohammed, J. Ahmad, *Pharmaceutics* **2023**, *15*, 1152.

[59] N. Handin, Proteomics informed investigation of human hepatocytes and liver tissue, **2021**.

[60] K. Pietrzak, A. Isreb, M. A. Alhnan, *European Journal of Pharmaceutics and Biopharmaceutics* **2015**, *96*, 380–387.

[61] H. Amekyeh, F. Tarlochan, N. Billa, *Frontiers in Pharmacology* **2021**, *12*, 646836.

[62] OpenAI, ChatGPT [Version GPT-3.5], [Modèle de langage], OpenAI, **2024**, https://openai.com/gpt-3.

[63] Poly(ethylene oxide) average Mv 100,000, powder 25322-68-3, http://www.sigmaaldrich.com/.

Chapter 7

Appendices

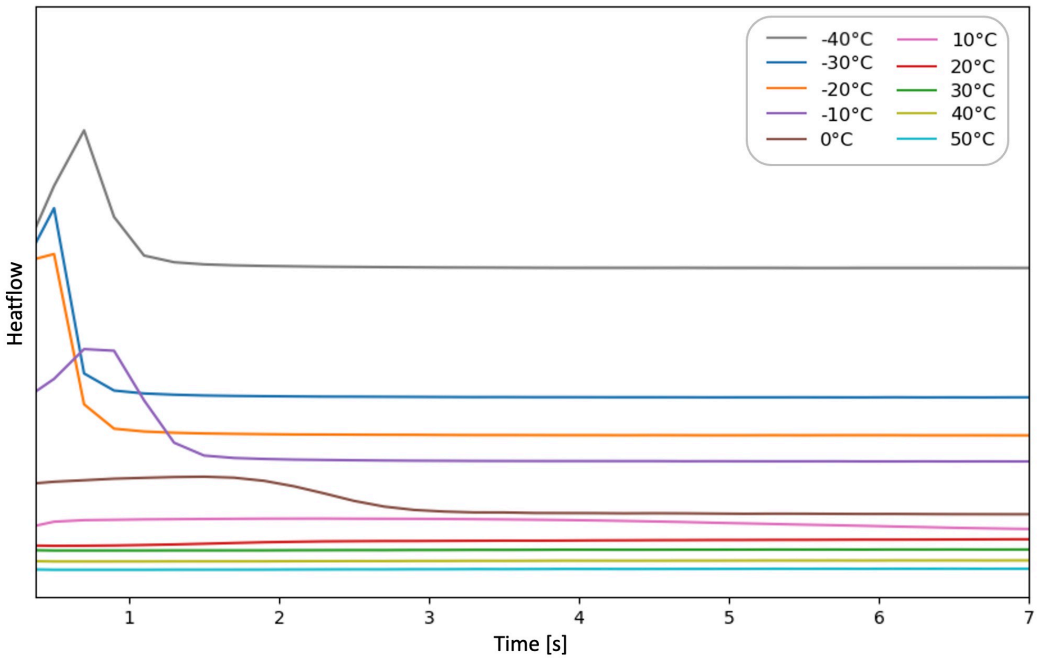

Figure 7.1: Isothermal fDSC curves of PCL/PEG 90/10 (the curves have been shifted vertically for clarity). This representation can be generalized to the other three blends (PCL/PEG 80/20, PCL/PEG 70/30 and PCL/PEG 50/50), as they behave in the same way.

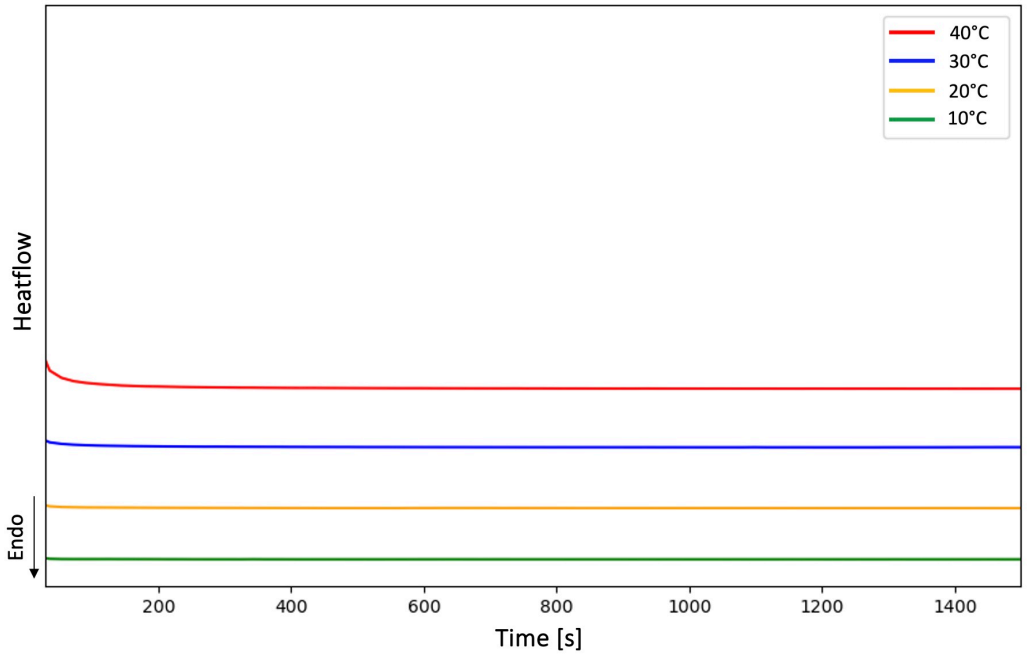

Figure 7.2: Isothermal DSC curves of pure PEG for T_{hold} between 40°C and 10°C by steps of 10°C (the curves have been shifted vertically for clarity).

UNIVERSITÉ CATHOLIQUE DE LOUVAIN
École polytechnique de Louvain
Rue Archimède, 1 bte L6.11.01, 1348 Louvain-la-Neuve, Belgique | **www.uclouvain.be/epl**